FINAL REPORT

No.2.

Project title:
GENERATION OF SPACE DEBRIS FROM EXPLOSIONS OF SPACECRAFTS' FUEL TANKS

Principal Investigator:
Nickolay N.Smirnov, Prof. Dr.Sc.-hab.(Phys.&Math.)
Head of Wave Process Labo ratory,
Dept. of Mechanics and Mathematics,
Moscow M.V.Lomonosov State University

Investigators:
Valery F.Nikitin, M.Sc.
Alexey B.Kiselev, Dr.Sc.-hab. (Phys.&Math.)
Irina D.Dimitrienko, Ph.D. (Phys.&Math.)
Vladislav R. Dushin, Ph.D. (Phys.&Math.)

A-1

Moscow - 1994

CONTENTS

	pages
Part 1. Introduction	3
Part 2. Propagation of detonation and deflagration waves with spherical symmetry	4
Part 3. A model of dynamic loading of the walls of spherical or cylindrical vessel for different scenario of combustion processes inside the vessel	11
3.1. Loading of walls in case of deflagration of a mixture	12
3.2. Loading of walls in case of reflection of normal detonation wave	13
3.3. Dynamic loading of the wall in case of reflection in DDT-zone	15
Part 4. Mathematical modelling of spherical fuel tanks fragmentation under the action of dynamic internal pressure	17
4.1. Problem statement on deforming a shell	17
4.2. Calculation of fragments' number	18
4.3. The guiding parameters of the problem	21
Part 5. Fragments acceleration by gas cloud propagating into vacuum	23
5.1. Problem statement and assumptions	23
5.2. Numerical model for gas cloud propagation and fragments motion	25
5.3. Obtaining the approximation formula	27
Part 6. Test cases, results and discussions.	29
Part 7. Conclusions	32
References	33
Figures	35
Appendix. User's instruction	68

Part 1. Introduction

The possible scenario of development of chemical explosion inside a closed vessel resulting in a breakup of the vessel were described in Preliminary report No.1. It was shown there that the type of breakup, the number and velocities of fragments are determined by the rates of energy release and wall pressure evolution inside the vessel. The results of breakup - mass and velocity distributions of fragments - would differ greatly depending on the combustion process inside the vessel: deflagration, detonation or deflagration to detonation transition (DDT).

To obtain a closed-form solution of the problem that can be compared with the existing experiments we'll try to concentrate our efforts on the solution for simple geometries: spherical and cylindrical vessels. The initial conditions will be also introduced in a form making it possible to obtain solutions posessing spherical or cylindrical symmetry.

The results of deflagration to detonation transition investigations [1.1] show that the process is complicated and the highest pressures and intensities of detonation waves are reached in the transition zone. This zone is characterized by the existence of overdriven detonation waves that slow down gradually to self-sustaining regime and the intensity of the waves decrease to that of normal detonation (close to Chapman-Jouget regime).

In case of central ignition of spherical or cylindrical volume of combustible gas there may occur different regimes that can produce different wall loadings after the reflection. If the DDT process does not take place inside the vessel the pressure rize and the wall loading is monotonous and it is determined by the rate of combustion. If the DDT process takes place inside the vessel rather far from the wall or there is a direct initiation of detonation the loading of the wall is determined by a reflected normal detonation wave. But in case the DDT - process takes place near the wall the pressure rize (wall loading) is determined by the reflection of an overdriven detonation wave that produces higher peaks of pressure. It is necessary to produce a closed form solution of the problem of wall loading, describing the multiplicity of scenario of DDT-processes that wouldn't be sophisticated and could be obtained within reasonable processor times. To solve the problem it is necessary in addition to the DDT investigations [1.1] that match the results of the experiments in tubes [1.2; 1.3] to examine some peculiarities of spherical and cylindrical deflagration and detonation waves propagation. Part 2 contains the results of these investigations.

The closed-form model of wall loading based on the results of investigations conducted taking into account the multiplicity of scenario of DDT-processes is described in Part 3.

Part 4 describes the results of breakup modelling under the influence of internal loading for different initial conditions and different scenario of combustion process inside the vessel. It is shown that the criterion of breakup can be determined from an independent experimental data.

The mathematical model of breakup takes into account the influence of temperature on the behaviour of the main parameters. It is shown, that the critical pressure of breakup changes depending on the type of combustion: the higher is the rate of loading - the higher turns to be the critical breakup pressure. The number of fragments is higher for higher pressures.

Part 5 presents the results of numerical modelling of fragments' acceleration in the expanding cloud of gaseous reaction products after the breakup. The numerical experiment conducted made it possible to work out approximation formulae determining final velocity of fragment depending on its shape, orientation, initial conditions and thermodynamic properties of the expanding gas.

Part 2. Propagation of detonation and deflagration waves with spherical symmetry

At deflagration or detonation initiation in premixed homogeneous combustible mixtures, for example by means of a spark or a detonator, a relatively small zone of raised values of parameters appears, this zone can be considered as a point source at a sufficient distance from the initiation location. Expanding products of detonator explosion in some cases can play the role of a spherical expanding piston.

Self-similarity of the problem on spherical detonation was established and the ordinary differential equations for describing the flow behind a wave front were derived in [2.1]. The case of the Chapman-Jouget spherical detonation was considered for example in [2.2, 2.3]. The most complete solution of the self-similar problem for cases of weak and strong detonation and Chapman-Jouget waves was obtained in [2.4]. In the present part profiles of flow parameters in propagation of spherical waves of strong and weak detonation and deflagration for cases of different velocities of piston motion from the initiation zone are investigated on the base of methods developed in [2.4].

We use the model where a detonation and deflagration waves zone is assumed to be a discontinuity surface, and suppose that detonation arises at time $t = 0$ in the symmetry center and propagates with a constant velocity; the initial mixture and reaction products are polytropic gases; Q_0=const is the specific heat of reaction. Combustible mixture is nonmobile ahead of the wave, and entropy of all particles has a constant value, and entropy increases for all particles by the same value in the detonation wave moving with constant velocity U i.e. a flow of detonation products within the continuity domain is homoentropic. Equations of nonstationary one-dimensional motion has the following form under these conditions:

$$\frac{\partial u}{\partial t} + u\frac{\partial u}{\partial r} = -\frac{1}{\rho}\frac{\partial p}{\partial r}; \tag{2.1}$$

$$\frac{\partial \rho}{\partial t} + u\frac{\partial \rho}{\partial r} + \rho\frac{\partial u}{\partial r} + \frac{2\rho u}{r} = 0; \tag{2.2}$$

where u, p, ρ - gas velocity, pressure and density respectively. Under these assumptions equations and boundary conditions allow an existence of self-similar solutions, i.e. solutions being functions only of one parameter $\xi = r/t$. Passing to self-similar variable ξ by the formulae:

$$\frac{\partial}{\partial t} = -\frac{\xi}{t}\frac{d}{d\xi}, \quad \frac{\partial}{\partial r} = \frac{1}{t}\frac{d}{d\xi}; \tag{2.3}$$

we reduce equations (1), (2) to the form:

$$\frac{du}{d\xi}(u - \xi) = -\frac{1}{\rho}\frac{dp}{d\xi}. \tag{2.4}$$

$$\frac{(u - \xi)}{\rho}\frac{dp}{d\xi} + \frac{du}{d\xi} + \frac{2u}{\xi} = 0. \tag{2.5}$$

Since the flow is homoentropic then $dp/d\xi = c^2 d\rho/d\xi$, where c is the sound velocity. Transform equation (5) to the form:

$$-\frac{1}{\rho}\frac{dp}{d\xi} = \left(\frac{du}{d\xi} + \frac{2u}{\xi}\right)\frac{c^2}{u - \xi} \tag{2.6}$$

and then substitute it into equation (4). We obtain:

$$\frac{du}{d\xi}[1-(\frac{u-\xi}{c})^2]=-\frac{2u}{\xi}. \tag{2.7}$$

It should be noticed that a constant flow (u=const) isn't a solution of equation (2.7) for the general case. Trivial solution of a constant flow i.e. $u \equiv 0$ (a quiescent state) is only possible.

Let us seek a non-trivial self-similar solution. Introduce new dependent variables

$$V \equiv \frac{u}{\xi}; \quad z \equiv \frac{c^2}{\xi^2}$$

and independent variable

$$\eta \equiv \ln(\frac{\xi}{U}).$$

On going to the new variables the system (2.6), (2.7) takes the form:

$$\Gamma(1-V)(V+\frac{dV}{d\eta})=2z+\frac{dz}{d\eta}. \tag{2.8}$$

$$\frac{V-1}{z\Gamma}(2z+\frac{dz}{d\eta})+\xi V+\frac{dV}{d\eta}=0; \tag{2.9}$$

where $\Gamma=\rho\frac{dc^2}{dp}=\frac{\rho}{c^2}\frac{dc^2}{dp}$. For polytropic gas $\Gamma=(\gamma-1)$, where $\gamma=c_p/c_v$ is the polytropic exponent. Resolving (8), (9) for the derivatives we obtain:

$$\frac{dz}{d\eta}=\frac{2z[z-(1-V)^2+\Gamma V(1-V)]}{(1-V)^2-z}. \tag{2.10}$$

$$\frac{dV}{d\eta}=V\frac{3z-(1-V)^2}{(1-V)^2-z}. \tag{2.11}$$

With the help of the system (2.10), (2.11) we determine $\frac{dz}{dV}=\frac{dz/d\eta}{dV/d\eta}$ and then write the expression derived in place of equation (2.10). Thus, the following system is derived:

$$\frac{dz}{dV}=\frac{2z}{V}\frac{z-(V-1)(\gamma V-1)}{3z-(1-V)^2}. \tag{2.12}$$

$$\frac{d\eta}{dV}=-\frac{1}{V}\frac{z-(1-V)^2}{3z-(1-V)^2}. \tag{2.13}$$

System (2.12), (2.13) can be solved sequentially: at first equation (12) gives the solution $z=z(V)$ and then the solution obtained is substituted into (13), from where $\eta=\eta(V)$ can be found.

Define boundary conditions for solving the equation (2.12) in the plane (V,z). For fixed t the condition $\xi=\xi(r)$ is satisfied. Consider the zone ahead of the detonation wave $B_0<r<A$ (Figure 2.1). In this zone $V=u_0/\xi\equiv 0$ (a quiescent zone). In this case ξ changes from $\xi_A=\infty$ for $r\to\infty$ to $\xi_{B_0}=R/t=U$ for $r=R=Ut$. Value of z within this zone changes from zero ($z_A=0$) for $\xi\to\infty$ to $z_0=c_0^2/U^2$ for $\xi_{B_0}=U$. On the plane (V,z) it corresponds to a trivial solution when a state changes from point A ($V=0$, $z_A=0$) to point B_0 ($V=0$, $z_0=c_0^2/U^2<1$) (Figure 2.2).

Parameters behind the detonation wave (point B_1) can be determined from the equations at the discontinuity front [2.5]:

$$\rho_1 w_1 = \rho_0 w_0,$$

$$p_1 + \rho_1 w_1^2 = p_0 + \rho_0 w_0^2, \tag{2.14}$$

$$e^{(1)}(T_1) + \frac{w_1^2}{2} + \frac{p_1}{\rho_1} = e^{(0)}(T_0) + Q_0 + \frac{w_0^2}{2} + \frac{p_0}{\rho_0},$$

$$w_i = u_i - U, \quad i = 0, 1;$$

these conditions for the problem considered at $V_0 = 0$ takes the form [2.4]:

$$\frac{\rho_0}{\rho_1} = 1 - V_1; \tag{2.15}$$

$$z_1 = \frac{\gamma_1^2}{(\gamma_1+1)^2}\left(1 + \frac{z_0}{\gamma_0}\right)^2 (1-\Lambda)(1+\gamma_1\Lambda); \tag{2.16}$$

$$V_1 = 1 - \left[\frac{\gamma_1}{\gamma_1+1}\left(1 + \frac{z_0}{\gamma_0}\right)(1-\Lambda)\right]; \tag{2.17}$$

where

$$\Lambda^2 = 1 - \frac{(\gamma_1^2-1)\left[\frac{2}{\gamma_0-1}z_0 + 1 + \frac{2Q_0}{U^2}\right]}{\gamma_1^2\left(1 + \frac{z_0}{\gamma_0}\right)}. \tag{2.18}$$

It follows from (2.16) and (2.17) that for fixed $\Lambda(U)$ the point B_1 in the plane (V, z) is on the parabola

$$z_1 = (1 - V_1)^2 \frac{1 + \gamma\Lambda}{1 - \Lambda}. \tag{2.19}$$

At the Chapman-Jouget detonation a relative gas velocity behind the wave is equal to the local sound velocity:

$$c_1^2 = w_1^2 = (u_1 - U_D)^2, \quad \Rightarrow \quad \left(\frac{c_1}{U_D}\right)^2 = z_1 = (V_1 - 1)^2.$$

Thus, the Chapman-Jouget detonation corresponds to the case $\Lambda = 0$ when the parabola (2.19) takes the form

$$z_1 = (1 - V_1)^2 \tag{2.19a}$$

and goes through the points (0,1) and (1, 0) (Figure 2.2).

For $\Lambda^2 > 0$, $U > U_D$ equation (2.18) has two roots: $\Lambda^+ > 0$, $\Lambda^- < 0$; $|\Lambda^-| = \Lambda^+$. It follows from equations (2.17) and (2.15) that $u_1^+ > u_1^-$, $\rho_1^+ > \rho_1^-$ i.e. the root $\Lambda^+ > 0$ corresponds to the case of strong detonation, and the root $\Lambda^- < 0$ corresponds to the case of weak detonation. Solution on the plane (V, z) can be prolonged either to the z axis (i.e. $V = 0$) that corresponds to the rest in the symmetry center or, at presence of a spherical piston, expanding with rate u_p, up to the line $V = 1$ as

$$V = \frac{u}{\xi} = \frac{u_p}{r_p/t}; \quad r_p = u_p t \quad \Rightarrow \quad V_p = 1.$$

In the zone between the piston and the detonation wave a shock wave can appear for which the same relations at a discontinuity surface (2.14) are true as for a detonation wave but with

conditions that there is no energy release due to a chemical reaction ($Q_0 = 0$) and a mixture composition doesn't change ($\epsilon^{(1)}(\bar{T}) \equiv \epsilon^{(0)}(\bar{T})$):

$$p_2(\bar{V}_2 = 1, z_2 = \rho_1(\bar{V}_1 = 1);$$

$$\bar{V}_2 = 1 + \frac{1 - z_2}{\gamma_1(\bar{V}_2 = 1)} = \bar{V}_1 = 1 + \frac{z_1}{\gamma_1(\bar{V}_1 = 1)};$$

$$(\bar{V}_2 = 1)^2 + \frac{2z_2}{\gamma_1 + 1} = (\bar{V}_1 = 1)^2 + \frac{2z_1}{\gamma_1 + 1}.$$

Consider the case of Chapman-Jouget spherical detonation wave propagation ($U = U_D$, $\Lambda = 0$). Since $\rho_1 > \rho_0$, it follows from equation (2.15) that $0 < V_1 < 1 - \rho_0/\rho_1 < 1$ and that the point B_1 ($V = V_1$, $z = (c_1/U_D)^2 < 1$) is on the left branch of parabola (2.19a). Passage from point B_0 to point B_1 in the plane (V, z) occurs by a jump (Figure 2.2). In the case when gas in the symmetry center is at rest ($u = 0$, $r = 0$) point M (Figure 2.1) in the plane (V, z) is on the axis $V = 0$: $M(V_M = 0, z_M = \infty)$. Point $K(V_K = 0, z_K = 1)$ is a singular point of the knot-type for equation (2.12). Thus, a solution connecting point B_1 with point M goes through point K. This point (non-material) moves on the plane (r, t) with the sound velocity:

$$z_k = \frac{c_k^2}{\xi^2} = 1 \Rightarrow \xi_k = c_k^2 = \frac{c_k^2}{t_k^2} \Rightarrow r = c_k t;$$

$$V_k = \frac{u_k}{\xi_k} = 0 \Rightarrow u_k = 0,$$

i.e. there is a characteristic on the plane (r, t) which bounds the rest domain (at this characteristic derivatives have discontinuity). Solution from point K to point M is rest: as in point K the condition: $u_k = 0$ is satisfied and in point M $u_M = 0$ due to symmetry, then the rest state satisfies the equations and the boundary conditions and due to uniqueness it is a solution between the points K and M. On the plane (V, z) states from $K(V_K = 0, z_K = 1)$ to $M(V_M = 0, z_M = \infty)$ are on the z axis from 1 up to ∞ (Figure 2.2). Thus, a desired solution behind the detonation wave consists of two branches: branch KM corresponds to the trivial solution $V = 0$, and branch KC_0B_1 to the solution of the general type for system (2.12), (2.13).

On the plane (r, t) a solution behind the detonation wave ($r = U_D t$) consists of the expanding domain of gas at rest ($u = 0, p = const = p_k$) and the rarefaction wave in the domain between the characteristic C_+^K: $r = C_K t$ and the detonation wave $r = U_D t$. This rarefaction wave isn't a solution of a simple wave. Along each axis $\xi = const$ values of flow parameters are constant.

Consider the case of strong detonation ($\Lambda = \Lambda^+ > 0$, $U = U_1 > U_D$), when gas goes from the state characterized on the (V, z) plane by point B_{01} to the state characterized by point B_{11} (Figure 2.2).

In this case point B_{11} characterizing parameters immediately behind the detonation wave is situated on parabola (2.19) which is higher then parabola (2.19a). Coordinates of point B_{11}: $V = V_{11}$ and $z = z_{11}$ can be determined from equations (2.16), (2.17) (Figure 2.2). In this case we can construct the solution where a compression wave propagates behind a detonation wave (it is an analog of a constant flow in a plane case) [2.5].

Continuous solution $B_{11}P_1$ (Figure 2.2) reaches the line $V = 1$, points of which can be considered as points corresponding to spherical pistons expanding with constant rate u_p. Point P_1, wherein the integral curve comes, defines the only velocity of the piston which corresponds to the given velocity of strong detonation wave U_1. With decreasing U_1 parameter Λ^+ diminishes, and $\Lambda^+ = 0$ at $U_1 = U_D$, parabola (2.19) transfers into parabola (2.19a) and point B_{11} becomes coincident with point B_1. Continuous compression wave is described by solution B_1P_D, the

piston velocity decreases to value u_{pD} i.e. we obtain a solution with the Chapman-Jouget detonation wave and the continuous compression wave behind the detonation wave front to the spherical piston moving with velocity u_{pD}.

On reducing the piston velocity so that a state ahead of the piston would correspond to point P_2 in Figure 2.2, we get the solution containing the Chapman-Jouget detonation wave, the rarefaction wave transforming gas from state B_1 into certain state C_0 on curve B_1C_0K, the shock wave transforming gas from state C_0 into state C_1 on curve B_1C_1K, and the continuous compression wave C_1P_2. Curve B_1C_1K presents a locus of states on the (V,z) plane which can be obtained as a result of a shock transition from the states lying on integral curve B_1C_0K.

With futher decreasing the piston velocity u_p coordinate z_p of point P grows up. In this case there is a solution wherein points C_1 and C_0 move along curves B_1C_0K and B_1C_1K and approach the point K. For $u_p = 0$ there is a solution containing Chapman-Jouget detonation wave, rarefaction wave and rest zone. Under the given boundary conditions (at the piston $u = u_p$ and at infinity) the constructed solution in the class of strong detonation and Chapman-Jouget detonation ($\Lambda \geq 0$) is unique.

Figure 2.3 shows computed results for the case of spherical detonation in mixture $Q_0 = 3 \cdot 10^6$ J/kg; $\gamma_0 = 1.4$; $\gamma_1 = 1.2$ in the form of dependence of pressure p/p_0 on non-dimensional coordinate r/R. Curve $B_0B_1C_0KM$ corresponds to the solution containing the Chapman-Jouget detonation wave B_0B_1 ($U_D = 1630$ m/s), the rarefaction wave and the rest zone at $u_p = 0$. Curve $B_0B_1C_0C_1P_2$ corresponds to the solution containing the Chapman-Jouget wave, the rarefaction wave, shock wave C_0C_1 and compression wave C_1P_2 at the expanding spherical piston velocity $u_p = 1200$ m/s. Curve $B_0B_1C_0'C_1P_2'$ is the pressure profile at decreasing the piston velocity u_p down to 1000 m/s. It is seen from the figure that futher decreasing the piston velocity will lead to reducing an intensity of secondary wave C_0C_1. Curve $B_0B_1P_D$ corresponds to the solution containing the Chapman-Jouget detonation wave and compression wave B_1P_D at piston velocity $u_p \sim 1320$ m/s.

Let us go to consideration of weak detonation ($\Lambda^- < 0$). In this case the problem solution isn't unique. An unique solution can be obtained in the weak detonation class when a value of one parameter on the detonation front is given in addition to the boundary conditions [2.4, 2.5], for example this parameter can be detonation wave velocity U_2 which defines uniquely $\Lambda_2^- < 0$ and point B_{12} on the (V,z) plane. Solution contains the rarefaction wave $B_{12}C_{02}K$ (Figure 2.2) and the expanding rest zone behind the weak detonation at $u_p = 0$. Pressure profile for the solution obtained at $U_2 = 1750$ m/s is shown in Fig.2.3 by curve $B_0B_{12}KM$. Solution at presence of a moving piston ($u_p = const > 0$) contains the rarefaction wave behind the detonation front from B_{12} to certain point C_{02} lying on integral curve $B_{12}C_{02}K$, the shock wave transforming the medium from state C_{02} into state C_{12} on curve $B_{11}C_{12}K$ and the continuous compression wave to state P ($V = 1$) ahead of the piston (Figure 2.2). Curve $B_{11}C_{12}K$ in Figure 2 is a locus of states which can be reached by a shock transition from states on curve $B_{11}C_{02}K$.

Figure 2.4 shows pressure profiles for the case of spherical weak detonation wave propagation with velocity $U_2 = 1750$ m/s. Curve $B_{01}B_{12}C_{02}KM$ corresponds to the case $u_p = 0$ when there exists a rest zone in the symmetry center. Solutions with an expanding spherical piston are represented by curves $B_{01}B_{12}C_{02}C_{12}P$ ($u_P = 1300$ m/s) and $B_{01}B_{02}C_{02}'C_{12}'P'$ ($u_p = 1000$ m/s). As seen from this figure, with increasing the piston velocity u_p an intensity of secondary shock wave $C_{02}C_{12}$ grows.

Solution of the indicated type for the case $\Lambda < 0$ exists not for all values of the boundary conditions but only till the piston velocity $u_p < u_{p1}(U_2)$, where $u_{p1}(U_2)$ is the piston velocity satisfying the solution with a strong detonation wave moving with velocity $U_1 = U_2$. Curve $B_{01}B_{12}B_{11}P_1$ in Figure 2.4 corresponds to a pressure profile for such limiting case (For the case considered $u_p = u_{p1}(U_2)$ =1500 m/s). At this piston velocity a secondary shock wave $C_{02}C_{12}$

overtakes a strong detonation wave $\bar{B}_{01}\bar{B}_{12}$, merges with that and forms a strong detonation wave $\bar{B}_{01}\bar{B}_{11}$ moving with the same velocity $U_1 = 1750$ m/s. For greater velocity of the piston $u_p \geq u_{p1}(U_2)$ a solution can be found only in the class of strong detonation. For this case a necessity to give an additional parameter at a detonation front is eliminated [2.5].

Solutions of analogical problems on detonation waves motion with the additional effect of a piston have been obtained for the plane one-dimensional case, for example in [2.5].

Consider the problem on spherical flame front propagation from a point source of initiation for the case when deflagration doesn't become detonation. Deflagration front is assumed to be a discontinuity surface, and then a solution is being sought within the scope of the same assumptions as in the previous problem. Consider the case when a weak deflagration front propagates with a given constant rate of normal burning W through an initial quiescent mixture with constant parameters. Normal burning rate W is subsonic with respect to gas ahead of the front, therefore a solution will contain a spherical shock wave moving ahead of a flame front. To find a solution in the disturbed zone of non-combusted gas between a shock wave and a deflagration front the system (2.12), (2.13) can be used with corresponding boundary conditions on the shock wave and on the deflagration front which have the following form in variables (V, z):

1) on the shock wave moving through quiescent medium ($V_0 = 0$) from (2.15)-(2.17) we have:

$$z_1 = (1 - V_1)(1 + \frac{\gamma_0 - 1}{2} V_1), \tag{2.21}$$

from where it is seen that shock waves transform the axis $V = 0$ into points of parabola (2.21);

2) on the flame front, behind which a state reaches the one at rest, parameters ahead of the front are connected by the relation:

$$z_2 = \frac{(1 - V_2)V_2\left(1 + \frac{\gamma_1 - 1}{2} V_2\right) + (\gamma_1 - 1)\frac{Q_0}{W^2}(1 - V_2)^3}{\frac{\gamma_1}{\gamma_0} - \frac{\gamma_1 - 1}{\gamma_0 - 1}(1 - V_2)}, \tag{2.22}$$

i.e. going onto the axis $V = 0$ through the flame front is possible only from points of curve (2.22). In deriving the equation (2.22) we use conditions (2.16), (2.17) at the discontinuity surface and the relation connecting a normal burning rate W and flame velocity U_F

$$U_F = \frac{W}{1 - V_2}.$$

Parameter γ_0 corresponds to the initial mixture, γ_1 corresponds to the combustion products.

The zone ahead of the shock wave images into the segment AH_0 on the (V, z) plane, where coordinates of point H_0 corresponding to the state ahead of the shock wave front are: $V_0 = 0$: $z_0 = c_0^2/U^2 < 1$. The state behind the shock wave corresponds to the point H_1 lying on parabola $z = z_1(V)$ (2.21) (Figure 2.5). Going from state H_1 into state N_2 ahead of the flame front lying on curve $z = z_2(V)$ (2.22) is realized within a continuous compression wave (Figure 2.5), and transition into state N_3 behind the flame front ($V_3 = 0$, $z_3 = c_3^2/U_F^2 > 1$) occurs by a jump. The rest zone behind the flame front images into ray N_3M. For this case a solution is unique at weak deflagration velocity W given.

Notice that points of curve (2.22), for which coordinate $z_2 < 1$ at point N_2, cannot correspond to the leading edge of the flame front, as that leads to supersonic flame front velocity with respect to gas behind the front (strong deflagration). For this case the solution can be constructed that contains the Chapman-Jouget deflagration wave and the rarefaction wave following the first one. State behind the deflagration wave should be situated on parabola $z = (1 - V)^2$, and a state ahead of the wave is on the curve:

$$z = \frac{\gamma_0}{\gamma_1}\left[\frac{\gamma_1^2 - \gamma_0}{\gamma_1(\gamma_0 - 1)} + \sqrt{\frac{(\gamma_1^2 - \gamma_0)^2}{\gamma_1^2(\gamma_0 - 1)^2} + \frac{2Q_0}{W^2}(\gamma_1^2 - 1) - 1}\right](1 - V)^2, \tag{2.23}$$

presenting a locus of states from which states on parabola (2.19a) can be reached on going through the flame front. The solution obtained contains the shock transition from the initial point on axis $V = 0$ into point H_{11} on curve (2.21), then the transition within a continuous compression wave to state N_{21} on curve (2.23), the jump in the deflagration wave to state F on parabola (2.19a) and the continuous transition within the rarefaction wave to point K (Figure 2.5). This picture supposes a presence of a zone of quiescent gas in the symmetry center. Depending on a location of point F on parabola (2.19a), further motion is possible either along integral curve FC_0K to point K or to singular point B ($z = \frac{3(\gamma_0-1)^2}{(3\gamma_0+1)^2}$, $V = \frac{2}{3\gamma_0+1}$) or to singular point C. For the second case the rest zone doesn't form, and the motion continues to the symmetry center and for the last case emptiness forms near the center. It is necessary to notice that there exists a solution for all points on parabola (2.21) higher than point Φ of parabolae (2.21) and (2.23) intersection. On parabola (2.19a) point Φ_1 corresponds to this point Φ and Φ_1 for the example considered is higher than point F_1, that says there are solutions with a rest zone for this case at absence of a piston.

Solution for weak deflagration ($W = 30$ m/s, $U = 500$ m/s) on the (z,V) plane is shown in Figure 2.6. Segment from O to H_0' corresponds to a quiescent initial combusible mixture zone. Jump to point N_1 occurs through the shock wave. Integral curve N_1N_2 corresponds to a continuous compression wave ahead of the flame front. Jump of parameters N_2N_3 occurs through the deflagration front. A rest zone begins directly behind the deflagration wave. Pressure profile corresponding to the solution obtained is shown by curve $H_0N_1N_2N_3$ in Figure 2.7.

Solution with the Chapman-Jouget deflagration wave ($W = 580$ m/s, $U = 800$ m/s) on the (z,V) plane in Figure 2.6 corresponds to segment OH_0 (a quiescent initial mixture), jump H_0L through the shock wave, compression wave LD, jump through deflagration wave DF, continuous rarefaction wave FK and the zone of quiescent gas. Corresponding pressure profile is shown in Figure 2.7 by curve H_0LDFK.

At presence of an expanding spherical piston for the Chapman-Jouget deflagration there are possible solutions with a compression wave instead of a rarefaction wave behind the deflagration front (integral curve FP in Figure 2.6) or with a rarefaction wave, a shock wave and compression wave by analogy with the considered flow pictures behind the Chapman-Jouget detonation front. For example Figure 2.7 shows a pressure profile for piston velocity $u_p = 580$ m/s (curve $H_0LDFC_0C_1P_1$).

Thus possible flow pictures at propagating deflagration and detonation waves with spherical symmetry have been investigated.

Part 3. A model of dynamic loading of the walls of spherical or cylindrical vessel for different scenario of combustion processes inside the vessel

One of the main parameters of the process is the energy of combustible mixture inside the vessel. Let us assume that the vessel contains a mixture of reagents and probably inert components. Y_i - mass concentration of reagents ($i = 1$ - oxidizer, $i = 2$ - fuel, $i = 3$ - inert components, $i = 4$ - reaction products); μ_i - molar masses of the components.

The brutto-reaction can be described by the formula:

$$\sum_{i=1}^{N} \nu_i' A_i = \sum_{i=1}^{N} \nu_i'' A_i; \tag{3.1}$$

where ν_i', ν_i'' - stoichiometric coefficients before and after the reaction respectively.

If chemical energy of combustion per mass unit of fuel is known (let it be ΔD) the specific energy release Q (chemical energy per mass unit of mixture can be determined as follows:

$$Q = \begin{cases} Y_2^* \Delta H; & \text{if } Y_1^* \geq \Phi Y_2^*; \\ Y_1^* \Delta H / \Phi. & \text{if } Y_1^* < \Phi Y_2^*; \end{cases} \tag{3.2}$$

where $\Phi \equiv \frac{\mu_1(\nu_1'' - \nu_1')}{\mu_2(\nu_2'' - \nu_2')}$ - stoichiometric ratio.

Let the total mass of gases inside a spherical vessel be M. For the case of cylindrical vessel let M be the mass of gas per unit length of a cylinder. The maximal equilibrium pressure p_m in the vessel after the combustion of mixture can be determined by a formula derived from the energy conservation law:

$$\frac{p_m}{p_0} = \frac{T_m}{T_0} \frac{\mu_0}{\mu_m} = \left(\frac{c_v^0}{c_v} + \frac{Q}{c_v T_0}\right) \frac{\mu_0}{\mu_m}, \tag{3.3}$$

where T_m - average temperature of mixture after combustion; c_v^0, c_v - specific heat of mixture before and after the reaction; μ_0, μ_m - molar masses of mixture before and after the reaction:

$$\mu = \left(\sum_{i=1}^{N} \frac{Y_i}{\mu_i}\right)^{-1}. \tag{3.4}$$

To obtain the closed form model of walls' loading it is necessary to examine different regimes of combustion process:

1. Deflagration wave propagates from the centre of symmetry to the walls (Regime No. 1).
2. Normal detonation wave reflects from the wall and produces impulse loading (Regime No.2).
3. DDT process takes place near the wall that causes the reflection of unsteady wave from the wall. This wave of unsteady structure can be weak and it can be very strong in case of overdriven detonation (Regime No.3).

One of the main characteristics of the DDT process is the predetonation length

$$L = L(p_0, T_0, r_0, \varkappa_j^T, \varkappa_j^i, \varkappa_j^{ch}, \ldots)$$

- the distance from the ignition point to the place of the onset of detonation. Experimental and theoretical investigations of DDT processes [3.1 - 3.14] in closed vessels and unbounded volumes showed that the predetonation length depends on many parameters: pressure (p_0), temperature

(T_0), chemical properties of mixture ($\varkappa_j^h$, $j = 1, 2, \ldots$), dimensions of a vessel (r_0), turbulent characteristics of a flow ($\varkappa_j^T$, $j = 1, 2, \ldots$), conditions of ignition and power of the source of ignition ($\varkappa_j^i$). Parameter L is of the type of parameters that can be measured much easier than calculated. This value will be one of the parameters of our model.

3.1. Loading of walls in case of deflagration of a mixture.

The Regime No.1 takes place in case dimensions of a vessel are rather small:

$$r_0 < L. \tag{3.5}$$

The velocities of flame propagation are subsonic and rather small in this case compared with sound velocity and it can be assumed that pressure has a nearly uniform distribution inside the vessel. The distribution of temperature will not be uniform since the central part of mixture combusts under low pressure conditions and is compressed then gradually to a high pressure p_m, and gas near the walls is compressed in advance before the combustion by expanding reaction products of internal volumes of mixture. The temperature rise in the last case will be smaller. The temperature rise due to adiabatic compression of unburnt gas can be determined by formula

$$\frac{T}{T_0} = \left(\frac{p}{p_0}\right)^{\frac{\gamma_0 - 1}{\gamma_0}}. \tag{3.6}$$

where $\gamma_0 = c_p^0/c_v^0$ - the ratio of specific heats.

The dependence of mass rate of combustion upon the pressure is given by formula [3.13 - 3.15]

$$\dot{m} = \rho v_f = \rho_0 v_{0\,l} \left(\frac{p}{p_0}\right)^{\frac{n}{\gamma}}, \tag{3.7}$$

where n is the reaction order. The formula (3.7) matches most of experiments when $n = 1$ [3.14].

Taking into account the compression of the unburned mixture in front of the flame zone and the mass burning rate (3.7) it is possible to obtain formulae [3.15] describing the pressure rise versus time in case of flame spread in a closed vessel:

1. for spherical symmetry

$$\tilde{t} = \int_1^{p/p_0} P^{-\frac{n}{\gamma}} \left[1 - P^{-\frac{1}{\gamma}} \frac{P_m - P}{P_m - 1}\right]^{-\frac{1}{n}} dP; \quad P = \frac{p}{p_0}. \tag{3.8}$$

$$\tilde{t} = t \cdot 4\pi r_0^2 \rho_0 v_0 (P_m - 1)/M;$$

2. for cylindrical symmetry

$$\tilde{t} = \int_1^{p/p_0} \frac{P^{-\frac{n}{\gamma}} dP}{\sqrt{1 - P^{-\frac{1}{\gamma}} \frac{P_m - P}{P_m - 1}}}; \tag{3.9}$$

$$\tilde{t} = t \cdot 2\pi r_0 \rho_0 v_0 (P_m - 1)/M.$$

The solutions of these equations in dimensionless variables for $n = 1$, $\gamma = 1,4$ are shown in Fig.3.1. In case of complete combustion of a mixture the upper limit of the integrals (3.8),

(3.9) is $\bar{P}_m = \frac{p_m}{p_0}$ determined by (3.3). Equations (3.8), (3.9) make it possible to determine $t_m = f(\bar{P}_m)$. The loading of the wall for the Regime No.1 can be determined by formula:

$$\frac{p_w}{p_0} = \begin{cases} \bar{P}(t), & \text{if } t \le t_m; \\ \bar{P}_m, & \text{if } t > t_m; \end{cases} \tag{3.10}$$

where $\bar{P}(t)$ and $\bar{P}_m$ are determined from (3.8), (3.9), (3.3).

3.2. Loading of walls in case of reflection of normal detonation wave.

Reflection of normal detonation wave takes place in case

$$\bar{L} < r_0 - l, \tag{3.11}$$

where l is the length of unsteady detonation wave propagation until it comes to a self-sustaining regime. The onset of detonation takes place at $t = \bar{L}$ and the pressure in the vessel at the time can be determined by formulae [3.15]:

$$\frac{\bar{L}}{r_0} = \left[1 - \bar{P}^{-\frac{1}{\gamma}} \frac{\bar{P}_m - \bar{P}}{\bar{P}_m - 1}\right]^{\frac{1}{3}}; \tag{3.12}$$

for the case of spherical symmetry, and

$$\frac{\bar{L}}{r_0} = \left[1 - \bar{P}^{-\frac{1}{\gamma}} \frac{\bar{P}_m - \bar{P}}{\bar{P}_m - 1}\right]^{\frac{1}{2}}; \tag{3.13}$$

for the case of cylindrical symmetry.

Corresponding time moments t_L can be determined from (3.8), (3.9). The time of reflection of the detonation wave from the walls t^* is estimated by formula

$$t^* = t_L + \frac{r_0 - \bar{L}}{D}. \tag{3.14}$$

where D is the detonation velocity for the mixture:

$$D = \frac{\sqrt{2(\gamma^2 - 1)Q} + \sqrt{2(\gamma^2 - 1)Q + 4\gamma p_0/\rho_0}}{2}. \tag{3.15}$$

At $t = t_*$ pressure on the wall goes up to p_r and then in time Δt it lowers down to the value p_{rD}, where Δt characterizes the reaction time in the detonation wave [3.16]:

$$\Delta t = k_0 Y_1^{-1} Y_2^{-1} \left(\frac{p_2}{p_0}\right)^{-1} \exp\frac{E}{RT}, \tag{3.16}$$

where E - activation energy of the chemical reaction. R - universal constant for gases. p_2, T_2 - pressure and temperature behind a leading shock wave propagating with the velocity D:

$$\frac{p_2}{p_0} = \left(\frac{2\gamma_0}{\gamma_0 + 1}\frac{D^2}{a_0^2} - \frac{\gamma_0 - 1}{\gamma_0 + 1}\right). \tag{3.17}$$

$$\frac{T_2}{T_0} = \frac{\left(\gamma_0 \frac{D^2}{a_0^2} + \frac{\gamma_0 - 1}{2}\right)\left(\frac{\gamma_0 - 1}{2}\frac{D^2}{a_0^2} + 1\right)}{\left(\frac{\gamma_0 + 1}{2}\right)^2 \frac{D^2}{a_0^2}}. \tag{3.18}$$

a_0 - sound velocity.

The value of Δt for hydrogen-oxygen mixtures is $\Delta t \sim 10^{-5}$ s and for dilute mixtures near the detonation limits it can reach $(1 \div 5) \cdot 10^{-4}$ s [3.16].

Pressures in the reflected detonation wave are determined by formulae:

$$\frac{p_r - p_0}{p_2 - p_0} = 1 + \frac{2\gamma}{(\gamma+1)\frac{p_2}{p_2} + (\gamma - 1)} \tag{3.19}$$

for the leading shock wave,

$$\frac{p_{rD}}{p_0} = \frac{p_D}{p_0} + \frac{\gamma+1}{4}\gamma\frac{\rho_D u_D^2}{\rho_0 a_0^2} + \sqrt{\frac{\gamma^2 \rho_D u_D^2}{\rho_0 a_0^2}\frac{p_D}{p_0} + \left(\frac{\gamma+1}{4}\gamma\frac{\rho_D u_D^2}{\rho_0 a_0^2}\right)^2}, \tag{3.20}$$

for the end of reaction zone.

The unknown values of pressure p_D, density ρ_D, velocity u_D at the end of reaction zone behind the detonation wave are determined by formulae:

$$\frac{u_D}{a_0} = \frac{1}{\gamma+1}\left(\frac{D}{a_0} - \frac{a_0}{D}\right), \tag{3.21}$$

$$\frac{\rho_D}{\rho_0} = \frac{D}{D - u_D}, \tag{3.22}$$

$$\frac{p_D}{p_0} = 1 + \frac{\gamma D u_D}{a_0^2} = 1 + \frac{\rho_0 D u_D}{p_0}. \tag{3.23}$$

The pressure near the wall p_{rD} decreases exponentially under the influence of rarefaction wave that follows the detonation one. The characteristic time of pressure decrease is that necessary for the last characteristic of the rarefaction wave to reach the wall:

$$\tau = \frac{\Delta r}{a_k}, \tag{3.24}$$

where Δr - the distance between this characteristic and the detonation wave, a_k - velocity of sound on this characteristic ($u_k = 0$). The solution obtained in part 2 shows that the ratio $\frac{\Delta r}{r_0} = k_c$ is a constant value very close to 0.5

$$\Delta r = k_c r_0 \approx 0.5 r_0. \tag{3.25}$$

The value of a_k can be determined approximately by formula:

$$a_k \approx \frac{D}{\gamma+1}\left(\frac{\gamma+1}{2} - \frac{a_0^2}{D^2}\frac{3-\gamma}{2}\right). \tag{3.26}$$

For strong detonation waves in gases under normal conditions $D \sim 2500 - 3000$ m/s, and $a_0 \sim 300$ m/s. That gives the ratio $a_0^2/D^2 \sim 0.01$, and formula (3.26) can be simplified

$$a_k \sim \frac{D}{2}.$$

Finally characteristic time τ is determined as follows

$$\tau = \frac{r_0}{D}. \tag{3.27}$$

3.3. Dynamic loading of the wall in case of reflection in DDT-zone.

This type of reflection takes place in case

$$r_0 - l < L < r_0. \tag{3.28}$$

The transition process starts after $r = L$ and that is why similar to Regime No.2 for the present regime we shall determine time t^*, pressure p^* from the solutions (3.8), (3.9). Investigations of the DDT-process [3.1-3.11, Preliminary Report 1] show that the intensity of detonation wave increases to that of an overdriven detonation and then decreases to the intensity of normal detonation. That is why the length of the DDT-zone l is the sum of two lengths:

$$l = l_1 + l_2, \tag{3.29}$$

l_1 - the length of formation of an overdriven detonation; l_2 - the length of slowing down the overdriven detonation to a self-sustaining mode.

The ratio of these lengths $l_1/l \approx 0.05 \div 0.5$.

To begin with let us reguard the situation

$$r_0 - l < L < r_0 - l_1. \tag{3.30}$$

For $t = t^*$ pressure on the wall rises to p'_r and then decreases up to p'_{vD} during the time $\Delta t'$. The pressure behind the detonation wave is determined taking into account that the wave propagates in an initially compressed media

$$\frac{p'_2}{p^*} = \frac{2\gamma}{\gamma+1}\frac{D^2}{a_*^2} - \frac{\gamma-1}{\gamma+1}, \tag{3.31}$$

where $p^* = p(t^*)$; $a_* = a_0\left(\frac{p^*}{p_0}\right)^{\frac{\gamma-1}{2\gamma}}$. Detonation velocity D determined by formula (3.15) also depends on initial parameters of mixture, but simple estimations show that the deviation of detonation velocity D from the initial value is negligibly small.

The velocity of the leading shock of such an intensity on entering the uncompressed mixture will be

$$D' = \sqrt{\frac{p'_2 - p_0}{\rho'_2 - \rho_0}\cdot\frac{p'_2}{\rho_0}}. \tag{3.32}$$

where

$$\frac{\rho'_2}{\rho^*} = \frac{\frac{p^*}{p'_2} + \frac{\gamma+1}{\gamma-1}}{\frac{\gamma+1}{\gamma-1}\frac{p^*}{p'_2} + 1}; \quad \frac{\rho^*}{\rho_0} = \left(\frac{p^*}{p_0}\right)^{1/\gamma}. \tag{3.33}$$

The Hugoniot curve gives two solutions for the detonation velocity $D' > D$ determined by (3.32). These solutions correspond to strong (overdriven) and weak detonation modes as it was discussed in Part 2. Gas velocity and pressure in the end of reaction zone are determined by formulae:

$$\frac{u'_D}{a_0} = \frac{1}{\gamma+1}\left[\left(\frac{D'}{a_0} - \frac{a_0}{D'}\right) \pm \sqrt{\left(\frac{D'}{a_0} - \frac{a_0}{D'}\right)^2 - \frac{2(\gamma^2-1)Q}{a_0^2}}\right], \tag{3.34}$$

$$\frac{p'_D}{p_0} = 1 + \frac{\gamma D' u'_D}{a_0^2}. \tag{3.35}$$

The solution with sign "+" in (3.34) corresponds to strong detonation and it must be used for this case.

The pressures on the wall after the reflection of an overdriven detonation wave are determined as follows:

$$\frac{p'_r}{p'_2} = \frac{p_0}{p_0} = 1 + \frac{2\gamma}{(\gamma+1)\frac{p_0}{p'_2} + (\gamma-1)}; \tag{3.36}$$

$$\frac{p'_{rD}}{p_0} = \frac{p'_D}{p_0} + \frac{\gamma+1}{4}\frac{\gamma\rho'_D u'^2_D}{p_0 a_0^2} + \sqrt{\frac{\gamma^2 \rho'_D u'^2_D}{p_0 a_0^2}\frac{p'_D}{p_0} + \left(\frac{\gamma+1}{4}\gamma\frac{\rho'_D u'^2_D}{p_0 a_0^2}\right)^2}; \tag{3.37}$$

$$\frac{p'_D}{p_0} = \frac{\bar{D}'}{\bar{D}' - u'_D}. \tag{3.38}$$

The decrease of pressure from p'_r up to p'_{rD} takes place during time interval $\Delta t'$:

$$\Delta t' = k_0 Y_1^{\gamma-1} Y_2^{\gamma-1} \left(\frac{p'_2}{p_0}\right)^{\gamma-1} \exp\left(\frac{\bar{E}}{RT'_2}\right); \tag{3.39}$$

$$\frac{T'_2}{T_0} = \frac{\left(\gamma_0 \frac{D'^2}{a_0^2} - \frac{\gamma_0-1}{2}\right)\left(\frac{\gamma_0-1}{2}\left(\frac{D'}{a_0}\right)^2 + 1\right)}{\left(\frac{\gamma_0+1}{2}\frac{D'}{a_0}\right)^2}. \tag{3.40}$$

For the case

$$r_0 - l_1 < L < r_0 \tag{3.41}$$

the parameters in the detonation wave and at the end of reaction zone can be described by approximate formulae:

$$p''_2 = -(p'_{2m} - p_m)\left(\frac{r - r_0}{l_1} + 1\right)^2 + p'_{2m}, \tag{3.42}$$

$$p''_D = -(p'_{Dm} - p_m)\left(\frac{r - r_0}{l_1} + 1\right)^2 + p'_{Dm}, \tag{3.43}$$

$$p'_{2m} = p'_2|_{L=r_0-l_1}; \qquad p'_{Dm} = p'_D|_{L=r_0-l_1}; \tag{3.44}$$

where functions p'_2 and p'_D are determined by (3.31), (3.35).

The wave velocity can be determined by (3.32), (3.33), the velocity of gas behind the wave u''_D can be determined as follows

$$\frac{u''_D}{a_0} = \frac{a_0}{\gamma \bar{D}''}\left(\frac{p''_D}{p_0} - 1\right). \tag{3.45}$$

The pressures on the wall after the reflection of detonation wave behind the reflected shock wave p''_r and at the end of reaction zone p''_{rD} can be determined from (3.36), (3.37), (3.38). Time interval $\Delta t''$ is determined from (3.39), (3.40).

For the last case ($r_0 - l_1 < L < r_0$) transition process starts near the wall and is not finished by the time of reflection. In fact, the new born wave does not enter fresh mixture. The flow disturbances during the stage of low velocity flame propagation have enough time to reach the wall. That is the reason we shall consider the wall loading for the times $t \le t^*$ to be the same as for the Regime No.1.

Part 4. Mathematical modelling of spherical fuel tanks fragmentation under the action of dynamic internal pressure.

To analyze causes and consequences of explosions of fuel tanks of last rocket stages on near-earth orbits there are first experiments on fragmentation of thin-walled shell structures under the action of internal explosion [4.1] and also attempts to solve the problem theoretically. In [4.2, 4.3] the simplest mathematical models are suggested that allow to calculate an average number of fragments, which are the result of breakup of thin cylindrical and spherical shells in explosion, and their initial velocity of scattering provided that all fragments have the same mass. This part deals with numerical modelling of thin-walled spherical shells fragmentation under the action of dynamic internal loading described in Part 3 taking account of fragments' distribution in terms of mass.

§4.1. Problem statement on deforming a shell.

The following assumptions on shell geometry and a character of its deforming and breakup are made:

1. The shell is thin: $h/r \ll 1$ (h - the thickness, r - the shell radius).

2. The effect of an internal dynamic load is modelled by pressure $p = p(t)$ depending on time and being uniformly distributed along the internal surface of the shell. Characteristic time of the load action $\bar{\tau} \gg h/a_0$ (a_0 is the sound speed in the shell).

3. The shell material is considered to be elastoviscoplastic and process of its deforming is adiabatic.

4. As a condition of the shell breakup beginning the entropic criterion of a limit specific dissipation [4.4] is assumed.

5. The shell breakup is assumed to occur as a result of the action of tensile ring stresses at the expense of consumption of elastic energy accumulated in the shell up to time $t = t_*$ of the breakup beginning; the work of external forces in breakup time is neglected; spalation fractures aren't considered [4.2, 4.3, 4.5].

Due to the first three assumptions the problem on deforming a thin shell can be considered as the one-dimensional spherical one.

Then the momentum equation has the form:

$$\rho\dot{v} = \frac{p(t)}{h} - 2\frac{\sigma_\theta}{r},$$

where ρ - density, v - radial velocity, r - current value of the shell radius, σ_θ - ring stress (the averaged stress over the shell thickness), a dot over a symbol means a material derivative with respect to time.

The rate of ring deformation is determined by:

$$\dot{\varepsilon}_\theta = \frac{v}{r},$$

other deformations are absent due to the shell thinness.

The equation of mass conservation has the form $\dot{\rho}/\rho = -2\dot{\varepsilon}_\theta$ from where we have:

$$\rho = \rho_0 \exp(-2\varepsilon_\theta),$$

where ρ_0 is the initial density.

State equations of elastoviscoplastic material are taken in the form [4.6.] which, taking account of

$$\bar{\sigma}_\theta \equiv \bar{\sigma} + \bar{S}_\theta, \quad \bar{\sigma}_\varphi \equiv \bar{\sigma}_\theta, \quad \bar{\sigma}_r \equiv \bar{\sigma} + \bar{S}_r \equiv 0, \quad 2\bar{S}_\theta + \bar{S}_r \equiv 0$$

for a spherical case, can be reduced to the form:

$$\dot{\bar{S}}_\theta \equiv \frac{2}{3}\mu\dot{\bar{\varepsilon}}_\theta = \frac{\mu}{\eta}\bar{S}_\theta\left(1 - \frac{J_0}{3|\bar{S}_\theta|}\right)H\left(1 - \frac{J_0}{3|\bar{S}_\theta|}\right),$$

$$\dot{\bar{\sigma}}_\theta \equiv 3\dot{\bar{S}}_\theta.$$

Here μ - shear modulus, η - dynamic viscosity of material, J_0 - static limit of elasticity in simple tension, $H(x)$ - the unit Heavyside function. Herewith the stress tensor σ_{ij} is divided into spherical $\sigma\delta_{ij}$ and deviator $\bar{S}_{ij}$ partials and it is assumed that rates of deformations can be divided into the rates of elastic and plastic ones and a plastic flow is incompressible:

$$\dot{\bar{\varepsilon}}_\theta \equiv \dot{\bar{\varepsilon}}^e_\theta + \dot{\bar{\varepsilon}}^p_\theta, \quad \dot{\bar{\varepsilon}}_\varphi \equiv \dot{\bar{\varepsilon}}_\theta, \quad \dot{\bar{\varepsilon}}_r \equiv \dot{\bar{\varepsilon}}^e_r + \dot{\bar{\varepsilon}}^p_r \equiv 0, \quad 2\dot{\bar{\varepsilon}}^p_\theta + \dot{\bar{\varepsilon}}^p_r \equiv 0.$$

Specific (per mass unit) elastic energy $\bar{E}$ and mechanical dissipation $\bar{D}$ can be determined by integration of the formulae:

$$\dot{\bar{E}} \equiv 2\frac{\bar{\sigma}_\theta}{\rho}\dot{\bar{\varepsilon}}^e_\theta, \quad \dot{\bar{D}} \equiv 2\frac{\bar{\sigma}_\theta}{\rho}\dot{\bar{\varepsilon}}^p_\theta.$$

Rates of elastic and plastic deformations are determined by the formulae:

$$\dot{\bar{\varepsilon}}^e_\theta \equiv \frac{\dot{\bar{S}}_\theta}{2\mu} + \frac{2}{3}\dot{\bar{\varepsilon}}_\theta, \quad \dot{\bar{\varepsilon}}^p_\theta \equiv \dot{\bar{\varepsilon}}_\theta - \dot{\bar{\varepsilon}}^e_\theta.$$

Calculation of the shell temperature in deforming for adiabatic approximation can be performed by the following procedure:

$$\rho c_\sigma \dot{\bar{T}} + 2\alpha_v \dot{\bar{S}}_\theta \bar{T} = 6\bar{S}_\theta \dot{\bar{\varepsilon}}^p_\theta.$$

Herein c_σ is the heat capacity at constant stresses, α_v is the coefficient of volumetric expansion [4.4].

Criterion of the shell breakup beginning is the entropic criterion of a limit specific dissipation that for the medium model considered is reduced to mechanical dissipation:

$$D|_{t=t_*} = D_*.$$

where D_* is the constant of limit specific dissipation determined with using the experiments on spalation fracture in a plane collision of plates [4.4].

§4.2. Calculation of fragments' number.

Fragments' number obtained in shell breakup can be found from the balance of elastic energy and work for breaking off a material. To describe fragments' distribution in terms of mass in explosive breaking of shells the Weibull distibution is most often used that is the special case of general probability distributions [4.7, 4.8]:

$$N(<m) = N_0\left[1 - \exp\left(-\left(\frac{m}{m_*}\right)^\lambda\right)\right]. \tag{4.1}$$

Here $N(\leqslant m)$ is the number of fragments with mass less than m; N_0 is the total number of fragments with mass more than 0 (a theoretical constant); m_* - the characteristic mass of distribution; Λ - the index of fragmentation quality.

For $\Lambda > 1$ distribution (4.1) is unimodal with the mode $M = m_*(1 - 1.\Lambda)^{1/\Lambda}$; for $\Lambda = 1$ this distribution becomes the exponential one; for $0 < \Lambda < 1$ it has an asymptote being the ordinate axis. Value of N_0 is finite at $\Lambda > 1$ and $N_0 = +\infty$ at $0 < \Lambda \leq 1$.

As shown in [4.7, 4.8], the unimodal distribution (4.1) describes satisfactorily spectra of breakup of metallic cylindrical shells of a medium-sized thickness ($h/r \simeq 0.1$). Better results can be given by the two-modal hyperweibul distribution suggested in [4.7] which includes two morphological collections: large fragments containing both shell surfaces (external and internal) and accompanying smaller fragments containing one of the surfaces.

For the case considered shells are very thin: $h/r \approx 0.001$ [4.1]. Therefore, evidently, we can restrict ourselves to unimodal distribution (4.1) and assume that all fragments contain both an internal surface and an external surface of the shell that is confirmed indirectly by experiments [4.1] conducted for such thin shells.

Let an area of an initial external Lagrangian surface of a fragment be equal to s, its internal surface be also equal to s (due to the shell thinness), and area of its lateral surface - $2ph$, where p is the semiperimeter of the contour s. The fragment mass is $m = \rho_0 hs$, therefore distribution in terms of mass (4.1) can be presented in the form of distribution in terms of areas s of fragments:

$$N(< s) = N_0\big[1 - \exp\big(-(\frac{s}{s_*})^{\Lambda}\big)\big]. \tag{4.2}$$

where $s_* = m_*/\rho_0 h$ is the characteristic area of the fragment.

Number of fragments with areas $s' \leq s \leq s''$ will be equal to:

$$N(s' \leq s \leq s'') = N_0\big[\exp\big(-(\frac{s'}{s_*})^{\Lambda}\big) - \exp\big(-(\frac{s''}{s_*})^{\Lambda}\big)\big].$$

Suppose now that from the total spectrum of the shell fragments with areas $0 < s < \pi d_0^2$ (d_0 is the initial diameter of the spherical shell) one can extract K groups of fragments with areas s_1, s_2, ..., s_k: $s_{min} < s_1 < s_2 < ... < s_K < s_{max}$, s_{min} and s_{max} are certain minimal and maximal areas of fragments. Let all fragments with areas $s_{min} \leq s \leq 0.5(s_1 + s_2)$ prove to be within the group of fragments with area s_1, all fragments with areas $0.5(s_1 + s_2) < s \leq 0.5(s_2 + s_3)$ prove to be within the group with area s_2, etc. up to the group with area s_k wherein there are fragments with areas $0.5(s_{k-1} + s_k) \leq s \leq s_{max}$.

Further in place of distribution (4.2) the following distribution will be used:

$$N(< s) = N_0\big[1 - \exp\big(-(\frac{s - s_{min}}{s_*})^{\Lambda}\big)\big], \quad s_{min} \leq s \leq s_{max}. \tag{4.3}$$

Then the number of fragments of the group s_j ($j = 1, 2, ..., K$) will be equal to

$$N_j = N_0(\beta_j - \beta_{j+1}), \qquad \beta_j = \exp\big(-(\frac{0.5(s_{j-1} + s_j) - s_{min}}{s_*})^{\Lambda}\big), \tag{4.4}$$

$$j = 1, 2, ..., K.$$

Here $s_0 = 2s_{min} - s_1$, $s_{K+1} = 2s_{max} - s_K$.

System (4.4) of K equations for calculation of the fragments' number of the groups can be complemented by the following two equations:

$$\sum_{j=1}^{K} s_j N_j = \pi d_0^2. \tag{4.5}$$

$$\sum_{j=1}^{K} \gamma h p_j N_j = \pi d_0^2 h \rho_0 \bar{E}_* k_E. \tag{4.6}$$

Equation (4.5) means that the summarized area of external surfaces of the fragments is exactly equal to the shell area, and equation (4.6) means that the elastic energy $\pi d_0^2 h \rho_0 \bar{E}_*$ ($\bar{E}_* \equiv \bar{E}|_{t=t_*}$) accumulated in the shell by time $t = t_*$ spends for formation of breakup surfaces. The coefficient k_E ($0 < k_E \leq 1$) of elastic energy consumption for formation of breakup surfaces is introduced into equation (4.6). Further it was assumed in calculations that all elastic energy spends for formation of breakup surfaces (i.e. $k_E = 1$). Herein γ is the specific energy, consumed for formation of the free surface unit, p_j is the semiperimeter of a fragment of the j-th group.

On using (4.5), the following equation can be derived from (4.6):

$$\sum_{j=1}^{K} N_j (p_j - \frac{\rho_0 \bar{E}_* k_E}{\gamma} s_j) \equiv 0. \tag{4.7}$$

To find $(2K+1)$ unknown variables p_j, N_j, N_0 there are only $(K+2)$ equations (4.4), (4.5) and (4.7). Select the following particular solutions of equation (4.7):

$$p_j = \frac{\rho_0 \bar{E}_* k_E}{\gamma} s_j, \quad j = 1, 2, \ldots, K. \tag{4.8}$$

Physical meaning of (4.8) consists in the following. One-half of energy necessary for formation of breakup surfaces around each j-th fragment with area s_j and mass m_j is extracted from mass m_j contained inside the fragment, and the second half - from the outside (from neighboring fragments). This is apparently a reasonable assumption.

The rest of $(K+1)$ equations (4.4), (4.5) can be easily solved now. At first we find:

$$N_0 = \frac{\pi d_0^2}{\sum_{j=1}^{K} s_j (\beta_j - \beta_{j+1})}, \tag{4.9}$$

and then according to (4.4) all N_j can be determined.

Notice that if we introduce the non-dimensional coefficient of shape $k_j = s_j / p_j^2$ [4.3], then we will obtain:

$$k_j = \frac{(\frac{\gamma}{\rho_0 \bar{E}_* k_E})^2}{s_j}. \tag{4.10}$$

For plane figures the shape coefficient changes within the limits

$$0 < k_j \leq 1/\pi. \tag{4.11}$$

provided that its maximal value is the one for a circle. As follows from (4.10), fragments of a greater area are less compact, that is verified by experiments on cylinders [4.8]. Small fragments can be considered as plane ones, therefore the following restriction from below on the fragments' area is derived from (4.11):

$$s_j \geq \pi (\frac{\gamma}{\rho_0 \bar{E}_* k_E})^2.$$

that is necessary to take into account when s_{min} is being chosen.

It should be noted that if the characteristic linear dimension of a fragment $l_j = 2s_j / p_j$ is introduced then it will prove to be that

$$l_j = \frac{2\gamma}{\rho_0 \bar{E}_* k_E}.$$

i.e. the characteristic linear dimension of all fragments groups is the same and coincident with the one obtained at solution of the problem when all fragments are assumed to be the same (solution [4.3]).

§4.3. The guiding parameters of the problem

For the considered problem on shell fragmentation there is a number of parameters which can be divided into two parts: parameters characterizing the shell material (ρ_0, μ, η, c_σ, α_v, J_0, γ, D_*) and parameters on which a distribution of fragments in terms of mass ($m_*(s_*)$, Λ) depends.

For the known constructional materials such parameters as density under the normal conditions ρ_0, shear modulus μ, heat capacity at constant stresses c_σ, coefficient of volumetric expansion α_v, static elasticity modulus in simple tension J_0 are table values. It is naturally that in deforming process with changing temperature T, density ρ, pressure, growth of plastic deformations these parameters also change. Flow limit J_0 and shear modulus μ are assumed to change in the deforming process according to the Steinberg-Guinan model [4.9]:

$$J_0 = J_0^0(1 + \beta\varepsilon_u^p)^n(1 - b\sigma(\frac{\rho_0}{\rho})^{1/3} - \chi(T - T_0)),$$

$$J_0^0(1 + \beta\varepsilon_u^p)^n \le J_{max},$$

$$\mu = \mu_0(1 - b\sigma(\frac{\rho_0}{\rho})^{1/3} - \chi(T - T_0)).$$

Here J_0^0, μ_0 are values of parameters under the normal conditions, $\varepsilon_u^p = 2|\varepsilon_\theta^p|$ is the intensity of plastic deformations; β, n, b, χ, J_{max} are constants of the material. These constants for many materials are presented in [4.9].

To determine dynamic viscosity of material η is more complicated. However, this parameter is also presented for many materials in the papers using the model of a solid deformable body quick-response to deformation rate (f.e. [4.6]).

Parameter γ (energy necessary for formation of the breakup surface unit) is also shown in a number of papers (see, for example, [4.7, 4.8]).

Now consider briefly determination of parameter D_* being limiting specific dissipation (criterion of the breakup beginning). As it was noted in §4.1, parameter D_* can be determined using the experiments on spalation breakup in plane collision of plates and numerical modelling of this process. It can be done by the following way.

In experiments a plane collision of two thin plates occurs: an impactor and a target (see, for example, typical experiments [4.10]). As a result of shock interaction of compression and tension waves, in the target under the certain conditions the region of tensile stresses expressed briefly appears, these stresses lead finally to formation of a spalation crack and in a number of cases also lead to a complete breakup of the target with withdrawal of a so-called spalation plate. Spalation formation becomes apparent in the graph of dependence of the velocity of the back target surface on time $w - t$ registered in the experiment. Such typical experimental dependence $w - t$ is shown in Figure 4.1 for the case of collision of aluminium impactor with titanium target for two collision velocities $V_0 = 660$m/s and $V_0 = 1900$m/s; solid curve corresponds to experiment [4.10], dashed curve - to computed results [4.4]. In a parallel way numerical modelling of collision of plates is conducted using computations with explicit separationof surfaces of spalation breakup of the target (in detail see [4.4]). In one of the experiments by means of varying the model parameters (in particular, the parametr D_*) the best coincidence of computed results with experiment is achieved, and the rest of experiments are used for control of parameter selection quality. Thus, for titanium in [4.4] the value $D_* = 75$ kJ/kg is chosen that allows to describe quite satisfactorily a number of experiments.

Character of fragments' distribution in terms of mass (area) is determined by two parameters: characteristic area s_* and indicator of crushing quality λ. These parameters should be chosen on the basis of the experimental data. Thus, for this objective experiments [4.1] will be used.

Part 5. Fragments acceleration by gas cloud propagating into vacuum.

This part of our investigations is denoted to obtaining the rate of final velocity of fragments formed by explosion of the fuel tank after breaking up its wall. Using some assumptions, we managed to reduce the number of dimensionless governing parameters of the problem to 4: gas adiabatic constant, relation of gas and fragment's densities, initial velocity of a fragment related to the Rayleigh sound velocity and the generalized drag coefficient. We made computations for spherical and cylindrical cases investigating the vast diapasone of parameters, obtained arrays of the final fragments velocities and then we managed to obtain high precision approximation formula connecting the final dimensionless velocity of a fragment with the 4 parameters mentioned above. To obtain then the real velocity one has only to multiply it by the Rayleigh sound velocity calculated for the initial parameters in the gas cloud.

5.1. Problem statement and assumptions.

We assume that the initial gas cloud is uniform and has a symmetrical shape (spherical or cylindrical). For it propagates into vacuum the disturbances in it decrease in the process and usually after reflecting from the wall propagate to the center not affecting the fragments originated from the broken wall so we assume that the nonuniformities of pressure in the initial gas can not affect heavily on the rate of the final results. However we must at first obtain the average rate of pressure and temperature in the initial gas. We do it according to the following formulae:

$$P_0 = \int_0^R r^\nu p dr \Big(\int_0^R r^\nu dr \Big)^{-1}, \qquad T_0 = \int_0^R r^\nu T dr \Big(\int_0^R r^\nu dr \Big)^{-1}, \tag{5.1}$$

where ν equals to 1 for cylindrical case and 2 for spherical one.

We assume the initial velocities in the gas equal to zero.

The main assumptions concerning the fragments are the following: we consider that the fragments affect on the gas much less than the gas affects on the fragments so we neglect the first effect. Then we neglect the fragments influence on each other. So we assume the fragments independent and not affecting the gas motion.

With these assumptions we obtain the following mathematical statement of the problem.

We will use the Lagrange's approach to the problem considering the mass of gas from the center or the axis to the fluid locus as the Lagrangian coordinate. This approach to gas dynamics is widely described in literature (f.e. in [5.1]). The Lagrangian mass coordinate here is determined as:

$$s = \int_0^r r^\nu \rho dr. \tag{5.2}$$

At first we introduce the dimensionless coordinates and variables according to the formulae:

$$p = P_0 \tilde{p},\ T = T_0 \tilde{T},\ E = E_0 \tilde{E},\ \rho = \rho_0 \tilde{\rho},\ r = R\tilde{r},\ s = S_0 \tilde{s},\ t = t_0 \tilde{t},\ v = V_0 \tilde{v}, \tag{5.3}$$

where p, T, E, ρ, r, s, t, v correspond to pressure, temperature, internal energy, density, radius (distance from the axis or the center), Lagrangian mass coordinate, time and velocity of the gas. The scaling rates P_0 and T_0 are considered to be the average pressure and temperature in the initial gas correspondingly determined in (5.1) and the other scaling rates are determined by the sequence of formulae:

$$\rho_0 = \frac{R_g P_0}{W T_0}, \quad V_0 = \sqrt{\frac{P_0}{\rho_0}} \quad t_0 = \frac{R_0}{V_0}, \quad S_0 = \frac{R_0^{\nu+1} P_0}{V_0^2}, \quad E_0 = \frac{P_0}{\rho_0}. \tag{5.4}$$

Here $R_g = 8.31\ J/(mol \cdot K)$ is the universal gas constant, μ is the average molar mass of gas and R_0 is the initial radius of the gas cloud. One can see from (5.4) that the velocity scaling rate is the Rayleigh sound velocity calculated for initial gas parameters.

Below we shall remove tilde upon letters in the formulae assuming all the parameters in the gas to be dimensionless if not specially mentioned.

We have the balances of mass, impulse and energy in the gas together with the state equation, the internal energy equation and the Euler's radius equation in the Lagrangian coordinate system (t, s):

$$\frac{\partial}{\partial t}(\frac{1}{\rho}) = \frac{\partial}{\partial s}(r^\nu v), \qquad \frac{\partial v}{\partial t} = -r^\nu \frac{\partial p}{\partial s}, \qquad \frac{\partial E}{\partial t} = -p\frac{\partial}{\partial t}(\frac{1}{\rho}),$$

$$p = \rho T, \quad E = \frac{T}{\gamma - 1}, \quad \frac{\partial r}{\partial t} = v. \tag{5}$$

Here γ is the gas adiabatic ratio assumed to be constant.

The boundary conditions are determined in the center or on the axis ($s = 0$) and at the edge of the gas cloud ($s = s_{max}$). As we forset that the gas propagates into vacuum the value of s_{max} is constant in the process. The value of s_{max} is determined accordingly to the determination of the Lagrangian mass variable (5.2):

$$s_{max} = \int_0^1 r^\nu \rho dr. \tag{5.6}$$

So we have the following boundary conditions to describe gas propagation into vacuum:

$$s = 0: \quad v = 0; \qquad s = s_{max}: \quad p = 0. \tag{5.7}$$

The initial conditions are simple according to our assumptions and the way of determining dimensionless values (5.3):

$$t = 0: \qquad v = 0, \quad p = 1, \quad T = 1. \tag{5.8}$$

We can see that the solution of the problem in general in dimensionless form depends only on the value of the adiabatic coefficient γ.

A fragment in the gas flow has the following laws of motion (in dimentional variables):

$$m\frac{du}{dt} = -\Sigma\delta\frac{\partial p}{\partial r}|_{r=x} - \frac{C_d}{2}S\rho|u - v|(u - v), \qquad \frac{dx}{dt} = u. \tag{5.9}$$

where:

$$S = \Sigma cos\alpha + (\delta + \frac{L^2}{4R_0})Lsin\alpha, \qquad C_d = C_d(\alpha, f), \quad f = L^2/\Sigma.$$

Here m is the fragment's mass, u is the fragment's velocity, Σ is the area of one side of the fragment, δ is the fragment's thickness, C_d is the drag coefficient (assuming the velocities high we neglect its dependance on the Reynolds number), S is the effective area facing the flow, α is the angle of fragment's orientation (zero if it is faced perpendicular to the flow), L is the effective size of the fragment, f is the shape coefficient. Here we assume the fragments originating from the thin membrane wall of the fuel tank with sizes much less than the diameter of the tank and the fragment's surface curvature radius equal to R_0.

The fragment in the flow rotates of course, but we shall assume that in its rotation the effective orientation to the flow o keeps its value. The shape coefficient f never changes in the process for one fragment, so we obtain that the value of the expression $(C_d S)/2$ in the second term of the impulse equation (5.9) is constant.

The initial conditions for the fragment in dimensional form are the following:

$$t = 0: \qquad u = u_0, \; x = R_0. \tag{5.10}$$

Using dimensionless variables and considering the scaling rate for x equal to R_0 and the scaling rate for u equal to V_0, we can rewrite the laws of motion (5.9) and the initial conditions (5.10) for fragments (removing tilde):

$$\frac{du}{dt} = -G\frac{\partial p}{\partial r}|_{r=x} - GB\rho|u - v|(u - v), \qquad \frac{dx}{dt} = u, \tag{5.11}$$

$$t = 0: \qquad u = U, \; x = 1, \tag{5.12}$$

The dimensionless numbers G, B and U correspond to densities ratio, generalized drag coefficient and dimensionless initial velocity, and are determined according to the following:

$$G = \frac{\Sigma\delta\rho_0}{m} = \frac{\rho_0}{\rho_f}, \qquad B = \frac{C_d S R_0}{2\Sigma\delta}, \qquad U = u_0\sqrt{\frac{\rho_0}{p_0}}. \tag{5.13}$$

The result we need to obtain is the value of fragment's velocity at the infinite time from the begining of the process, so it is independent of the time scale. We will note it $\tilde{u}_\infty$ (dimensionless) or u_∞ (dimensional). To obtain the dimensional velocity we must multiply dimensionless one by V_0 (Rayleigh sound velocity for the initial gas parameters).

So using our assumptions we reduced the set of parameters affecting the dimensionless final result to γ, G, B, and U. Below we will describe the computational model obtaining arrays of $\tilde{u}_\infty$ and finally the approximation formula taking into account these four parameters.

5.2. Numerical model for gas cloud propagation and fragments motion.

To calculate the gas motion the numerical model was used described in [5.1]. We used the differential network of $N = 513$ nodes $\{s_k\}$, $k = 0, \ldots, N-1$, each node corresponding to a definite value of Lagrangian mass coordinate. The network was built uniform relatively to the initial state of Eulerian radius (non-uniform relatively to the Lagrangian coordinate). We used implicit scheme to approximate the gas dynamics equation and a "plain iteration" technique to solve the problem on each step of time.

Actually, the transfer from the n-th to $n+1$-th time layer is obtained from the equations (5.5), boundary conditions (5.7) and initial conditions (5.8) and looks like:

$$\frac{v_k^{n+1} - v_k^n}{\tau_n} + \frac{R_k}{h_k + h_{k-1}}(p_k^{n+1} - p_{k-1}^{n+1} + p_k^n - p_{k-1}^n) = 0, \quad k = 1, \ldots, N-1$$

$$\frac{r_k^{n+1} - r_k^n}{\tau_n} - 0.5(v_k^{n+1} + v_k^n) = 0, \quad k = 0, \ldots, N-1$$

$$\frac{1/\rho_k^{n+1} - 1/\rho_k^n}{\tau_n} - \frac{0.5}{h_k}(R_{k+1}(v_{k+1}^{n+1} + v_{k+1}^n) - R_k(v_k^{n+1} + v_k^n)) = 0, \quad k = 0, \ldots, N-2$$

$$E_k^{n+1} - E_k^n + 0.5(p_k^{n+1} + p_k^n)(1/\rho_k^{n+1} - 1/\rho_k^n) = 0, \quad k = 0, \ldots, N-2$$

$$\bar{R}_k \equiv \begin{cases} ((r_k^{n+1})^2 + r_k^{n+1} r_k^n + (r_k^n)^2)/3, & \nu = 2. \\ (r_k^{n+1} + r_k^n)/2, & \nu = 1. \end{cases} \quad k = 0, \ldots, N-1$$

$$\bar{T}_k^{n+1} = \bar{E}_k^{n+1}(\gamma - 1), \quad p_k^{n+1} = \bar{T}_k^{n+1} \rho_k^{n+1}, \quad k = 0, \ldots, N-2 \tag{5.14}$$

Here the values of v_k, r_k, $\bar{R}_k$ are calculated in the k-th node s_k of the differential scheme, the other values are calculated between s_k and s_{k-1}. $h_k = s_{k+1} - s_k$. τ_n is the timestep value.

In order to supress oscillations we use artificial Neumann's viscosity, adding it to pressure in the impulse equation: it is calculated by the sequence of formulae between s_k and s_{k+1} according to [5.1]:

$$d_v = \frac{v_{k+1}^{n+1} - v_k^{n+1}}{h_k}, \qquad d_r = \rho_k^{n+1} \begin{cases} (r_{k+1}^{n+1} + r_k^{n+1})/h_k, & \nu = 1. \\ ((r_{k+1}^{n+1})^2 + (r_k^{n+1})^2)/h_k, & \nu = 2. \end{cases}$$

$$\omega_k^{n+1} = \frac{5(\gamma - 1)}{N^2} \begin{cases} d_v d_r, & d_v < 0. \\ 0, & d_v > 0. \end{cases} \tag{5.15}$$

The boundary conditions in the differential scheme are:

$$v_0^{n+1} = 0, \quad p_{N-1}^{n+1} = 0, \quad \omega_{N-1}^{n+1} = 0. \tag{5.16}$$

The initial conditions:

$$v_k^0 = 0, \quad p_k^0 = 1, \quad T_k^0 = 1, \quad E_k^0 = 1/(\gamma - 1), \quad k = 0, \ldots, N-1 \tag{5.17}$$

The algorithm realising the scheme (5.14-5.17) is described in [5.1]. We used the simplest techniques of "plain iteration": it requires the modified Courant criterium for the timestep rate. Actually we used the criterium taking the Neumann's viscosity and possibility of breaches into account:

$$\tau^n < \begin{cases} k > 0: & 0.2(r_{k+1}^{n+1} - r_k^{n+1})/a_k, \\ k = 0: & 0.2 r_1^{n+1}/a_0 \end{cases} \quad \text{where}$$

$$a_k = \begin{cases} \sqrt{\left(\frac{p_{k+1}^{n+1} + \omega_{k+1}^{n+1}}{p_k^{n+1} + \omega_k^{n+1}}(\gamma + 1) + \gamma - 1\right)\frac{p_k^{n+1} + \omega_k^{n+1}}{2\rho_k^{n+1}}} + max\{v_k^{n+1}, v_{k+1}^{n+1}\}, & \frac{p_{k+1}^{n+1} + \omega_{k+1}^{n+1}}{p_k^{n+1} + \omega_k^{n+1}} > 1. \\ \sqrt{\left(\frac{p_k^{n+1} + \omega_k^{n+1}}{p_{k+1}^{n+1} + \omega_{k+1}^{n+1}}(\gamma + 1) + \gamma - 1\right)\frac{p_{k+1}^{n+1} + \omega_{k+1}^{n+1}}{2\rho_k^{n+1}}} + max\{v_k^{n+1}, v_{k+1}^{n+1}\}, & \frac{p_{k+1}^{n+1} + \omega_{k+1}^{n+1}}{p_k^{n+1} + \omega_k^{n+1}} < 1. \end{cases} \tag{5.18}$$

To calculate the fragments motion we used the "predictor-corrector" techniques, or the modified Euler techniques of the second order approximation [5.2]. We calculated the fragments motion on each step of time after calculating gas motion, so we used the same rate of timestep. As the fragments do not affect gas and each other in our model, we treated a big number of fragments with different parameters simultaneously.

Actually to obtain arrays of $\tilde{u}_\infty$ we examined the following diapasones of parameters: $G = 10^{-4} \div 10^{-2}$, $B = 10 \div 1000$, $U = 0 \div 1$. There were 7 values of parameters taken from each diapasone including the lowest and the highest value, so 343 model fragments were examined in each calculation. Actually the set of values used in calculations looks like:
$G_i = \{1 \cdot 10^{-4}, 2 \cdot 10^{-4}, 5 \cdot 10^{-4}, 1 \cdot 10^{-3}, 2 \cdot 10^{-3}, 5 \cdot 10^{-3}, 1 \cdot 10^{-2}\}$.
$B_j = \{10, 20, 50, 100, 200, 500, 1000\}$.
$U_k = \{0, 1/6, 2/6, 3/6, 4/6, 5/6, 1\}$.

The calculation itself depended also on the value of γ and on the type of geometry (spherical or cylindrical), i.e. on ν. So we made calculations for $\gamma_m = \{1.20,\ 1.25,\ 1.33,\ 1.40\}$ and for both geometries obtaining in each case array of $\tilde{u}_\infty$ values.

5.3. Obtaining the approximation formula.

Such a low number of dimensionless parameters makes it possible to try to obtain approximation formula for $\tilde{u}_\infty$: usage of this formula can save calculations time. This formula needs to be precise enough in the diapasone of parameters mentioned above.

To obtain the formula we used minimal squares techniques, however slightly modified. Let us involve the following notation:

$$\tilde{u}_\infty^{calc} = V_{\nu,\gamma_m}^{i,j,k}, \qquad \tilde{u}_\infty^{appr} = W(\nu, \gamma_m, G, B, U),$$

where the first term is the calculated array, indexes i, j, k correspond to the values of G_i, B_j, U_k used in calculations, and the second one is the approximative function we need to obtain. The minimal squares techniques requires us to minimize the functional:

$$\Phi = \sum_{i=0}^{6}\sum_{j=0}^{6}\sum_{k=0}^{6}\left(\frac{V_{\nu,\gamma_m}^{i,j,k} - W(\nu,\gamma_m,G_i,B_j,U_k)}{V_{\nu,\gamma_m}^{i,j,k}}\right)^2.$$

For we have calculated the array V for certain values of γ and ν, then we need to suggest a set of W formulae for these values.

We suggest the following formula consisting of 10 coefficients:

$$W = U + \frac{C_0GB + C_1G}{1 + \dfrac{C_3GB + C_4G + C_5U}{1 + C_6GB + C_7G + C_8U}} \cdot \frac{1}{1 + \dfrac{C_2U}{1 + C_9U}}.$$

We have solved the problem of Φ value minimization for the values of γ and ν mentioned above. As the minimum is close to zero, then to find the values of C_n array with maximal precisity we actually minimized not Φ itself but:

$$\Psi = \begin{cases} \log\Phi, & \Phi < 1, \\ \Phi - 1, & \Phi > 1. \end{cases}$$

We applied the heavy ball techniques to obtain the minimum of Ψ [5.2]. The techniques of gradient slide [5.2] here is less available, for the 10-dimensions Ψ hypersurface has narrow gaps and therefore the gradient slide requires much more steps to find the minimum. In order to optimize the process of minimization the friction coefficient was different for different directions and it raised automatically with oscillations of the "ball".

Our results are shown in the tables 1-2.

γ	1.40	1.33	1.25	1.20
C_0	3.5353e-1	3.5904e-1	3.6555e-1	3.6976e-1
C_1	1.6002e+0	1.6386e+0	1.6843e+0	1.7141e+0
C_2	-2.4429e-1	-2.3536e-1	2.1388e-1	-2.0892e-1
C_3	2.5589e-1	2.5336e-1	2.4998e-1	2.4783e-1
C_4	1.4080e+0	1.4509e+0	1.4905e+0	1.5274e+0
C_5	1.5722e+0	1.5319e+0	1.4873e+0	1.4571e+0
C_6	1.5237e-2	1.6111e-2	1.7191e-2	1.7978e-2
C_7	1.1635e+0	1.2033e+0	1.1843e+0	1.2075e+0
C_8	-6.0898e-1	-5.8532e-1	-5.5738e-1	-5.3848e-1
C_9	5.2481e+0	4.9598e+0	4.0670e+0	3.9471e+0
Φ	4.95e-4	5.19e-4	5.63e-4	5.95e-4

Tabl.1. Coefficients for spherical case ($\nu = 2$).

γ	1.40	1.33	1.25	1.20
C_0	4.8919e-1	4.9544e-1	5.0267e-1	5.0726e-1
C_1	1.7300e+0	1.7688e+0	1.8123e+0	1.8410e+0
C_2	-1.6851e-1	1.6529e-1	1.5920e-1	1.5546e-1
C_3	3.1189e-1	3.0727e-1	3.0166e-1	2.9786e-1
C_4	1.5203e+0	1.5593e+0	1.5791e+0	1.6160e+0
C_5	1.2600e+0	1.2203e+0	1.1730e+0	1.1426e+0
C_6	1.7082e-2	1.8213e-2	1.9654e-2	2.0694e-2
C_7	1.1118e+0	1.1133e+0	1.1252e+0	1.1310e+0
C_8	-5.2095e-1	-4.9499e-1	-4.6385e-1	-4.4332e-1
C_9	2.4764e+0	2.4672e+0	2.3980e+0	2.3645e+0
Φ	9.28e-4	9.93e-4	1.08e-3	1.14e-3

Tabl.2. Coefficients for cylindrical case ($\nu = 1$).

It can be noticed from the tables 1-2, that the precisity of approximation is high so that the rate of relative precisity of 1% in the examined diapasone of parameters is guaranted (actually the precisity is much higher).

To obtain the approximation formula taking γ into account we use the Lagrangian polynom, so that if W_m is calculated for γ_m according to the table 1 or 2, the value of W for γ is calculated (see [5.2]):

$$W = \sum_{m=0}^{3} \frac{\prod_{j=0, j\neq m}^{3} (\gamma - \gamma_j)}{\prod_{j=0, j\neq m}^{3} (\gamma_m - \gamma_j)} W_m.$$

This approximation formula is the main result of this part of our report. It can significantely simplify the calculations. To obtain the dimensional value of the fragment's final velocity one can multiply W by the value of Rayleigh sound velocity calculated for the average initial parameters in gas:

$$a_\infty = W \sqrt{\frac{P_0}{\rho_0}}.$$

Part 6. Test cases, results and discussions.

The tests of the theoretical model developed were performed for the cases of detonation propagation in hydrogen-oxygen mixture in a cylindrical container with thin walls. The parameters of the container and the mixture were chosen corresponding to the experiments described in [4.1]. Since the initial pressure in the tank is not so high it was considered that at the initial instant ($t = 0$) the shell is elastic. Under this assumption the initial conditions ($t = 0$) for the shell are the following:

$$v = 0: \quad \sigma_\theta = \frac{p_0 r_0}{2h}; \quad S_\theta = \frac{\sigma_\theta}{3}; \quad \varepsilon_\theta = \varepsilon'_\theta = \frac{\sigma_\theta}{2\mu};$$

$$\varepsilon''_\theta = 0: \quad w = r_0 \varepsilon_\theta; \quad r = r_0 + w;$$

$$E = \mu\left[1 + \exp(2\varepsilon_\theta)(2\varepsilon_\theta - 1)\right]/\rho_0;$$

$$D = 0: \quad \rho = \rho_0(-2\varepsilon_\theta),$$

where r_0 - initial radius of the shell; w - displacement.

Taking into account the restrictions on the minimal fragments' area obtained in §4.3 we assume that for the smallest fragments their area is $s_1 = 2\pi\left(\frac{1}{\rho_0 E}\right)^2$.

Totally $K = 20$ groups of fragments were reguarded in the model. The areas were equal to $s_j = s_{j-1} \cdot 10^{0.25}$, $j = 2, 3, ...20$. The properties of the materials of the shell were the following: ρ =2700 kg/m^3; μ = 27 GPa; c_σ = 924.3 J/kg· K; $\alpha_\mu = 6.72 \cdot 10^{-5}$K^{-1}; $J_0 = 0.29$ GPa; $J_{max} = 0.68$ GPa; $\beta = 125$; $b = 0.065$GPa^{-1}; $\lambda = 6.2 \cdot 10^{-4}$K^{-1}; $n = 0.1$.

The data on chemical properties of combustible mixture inside the tank, energy release, combustion rate, activation energies and DDT process is shown in the table Fig.6.1. The data corresponds to the hydrogen-oxygen mixture similar to that used in the experiment ESOC-2 [4.1].

Initial conditions, geometry of a fuel tank and physical properties of material are shown in the table Fig.6.2. Recalculated properties of mixture: initial and final equilibrium states - are shown in the Fig.6.3. The key parameters of detonation wave propagation and its reflection from the walls both for cylindrical and spherical tanks for the given initial and boundary conditions are shown in the Fig.6.4.

The pressure - time diagram of wall loading is shown in the Fig.6.5. It should be mentioned separately that initial time ($t = 0$) on the diagram for the case of detonation corresponds to the moment of the onset of detonation and not to the time of ignition as it can be easily seen from the table (Fig.6.4).

The key parameters of the shell under the influence of the loading are shown in the table (Fig.6.6). It is seen that both for cylindrical and spherical shells the fragmentation occurs under such conditions.

The Fig.6.7 shows the diagram of the total number of fragments of different mass originating as a result of breakup of a cylindrical and spherical shell. The total number of fragments for cylindrical case is larger than that for a spherical one due to the particular length/radius ratio for the cylinder (see Fig.6.2) that gives a larger surface in comparison with a sphere of the same radius. The experimental results on distributions of fragments' number versus mass are shown in the Fig.6.8 (experimental data [4.1]). Comparison of the results shows that for the part of spectrum containing large fragments coincidence is rather fine. A slight difference for small fragments (theory gives a larger number than the experiment) can be

explained by the fact that in course of the experiments not all the fragments were collected. It is mentioned in [4.1] that for the test case ESOC-2 1.3% of the total mass was lost that equals about 20 grams. The existing difference of mass for small fragments in theoretical and experimental results is much less than that value.

The plots of final velocity of fragments versus mass for different angles of orientation of fragments are given in the Fig.6.9. The coincidence of final velocities and breakup velocities of fragments (Fig.6.6) with the experimental data [4.1] is also fine.

The Fig.6.10 shows the total momentum distribution of fragments versus mass for cylindrical and spherical cases for different angles of orientation.

To demonstrate the influence of the type of the process of energy release inside the tank the next set of figures illustrates the breakup of the same fuel tank in cases the pure combustion (deflagration) takes place inside the tank (Figs.6.11-6.16) and deflagration to detonation transition takes place near the walls of the tank (Figs.6.17-6.22). For the last case an overdriven (strong) detonation wave reflects from the wall and pressure after the reflected wave is higher (Figs.6.17, 6.18) than in case of normal detonation (Figs.6.4, 6.5). The wall loading for DDT process differs for cylindrical and spherical cases (Fig.6.18). As a result a larger amount of elastic energy is stockpiled by the time of breakup (Fig.6.19) and the number of fragments increases (see Fig.6.20). Maximum number of fragments is moved in the direction of smaller masses (Fig.6.20) both for cylindrical and spherical cases. The final velocity of fragments (Fig.6.21) is higher than in case of normal detonation and it doesn't depend practically on the orientation o a fragment. Total momentum of fragments also turns to be higher (Fig.6.22).

For the case of deflagration wave propagating inside the tank the final equilibrium pressure in the tank is the same as for detonation but it needs a longer period to reach this pressure (Fig.6.12). The results show that by the time of breakup elastic energy stockpiled by the wall is nearly the same as that for the case of normal detonation (Fig.6.13). That leads to practically the same fragmentation picture (Fig.6.14). But final velocities of fragments (Fig.6.15) are less than in case of normal detonation. Orientation angle of fragment in the expanding stream of reaction products plays a more important role for this case. Total momentum of fragments after the breakup is less than in case of normal detonation (Fig.6.16). The results show that the angle of orientation of fragments in the expanding reaction products plays the most important role for the case of slow loading (deflagration) (Fig.6.16), plays smaller role in case of normal detonation (Fig.6.10) and practically doesn't influence the results for the case of overdriven detonation reflection in DDT process (p.6.21).

The results of numerical modelling show that the breakup process, the number and mass distribution of fragments, and their velocities differ greatly depending on the rate of energy release inside the tank and this dependence is not monotonous. For the lowest (deflagration) and highest (detonation) rates of energy release the number of fragments is less than for the medium rate of energy release: i.e. deflagration to detonation transition. Maximal fragments' velocities and the time before the breakup for those three cases are illustrated by the following table for cylindrical symmetry.

Parameter	Deflagration	Transition process	Detonation
breakup time (ms)	7017	4272	1029
maximal velocity (m/s)	900	2500	1000

This dependence of breakup characteristics on the rate of the energy release inside the fuel tank is too large to be neglected as it was usually done before.

The next series of numerical experiments was devoted to testing the so-called "similarity parameters" for breakup of fuel tank [4.1]. The similarity parameter was supposed to be $p_0 r_0/h \equiv A \equiv$const. It was supposed in [4.1] that for the constant values of similarity parameters the number of fragments and their final velocities remained constant and masses of large fragments grow up proportionally to the growth of the volume of a shell's material.

Figs. 6.23, 6.24 present the results of calculations for the case similar to ESOC 2 but with proportionally increased radial dimensions of the shell and thickness: $r_0 = 130$ sm; $h = 2$ mm. (In case ESOC 2 we had $r_0 = 30$ sm; $h = 0.5$ mm). This increase of dimensionsof the tank preserves the similarity parameter A constant. It can be seen from Fig.6.23 that the number of fragments increased essentially contrary to predictions. The increase of final velocity is more than 20% (see Fig.6.24). Small fragments have more strong dependence of velocity on the orientation angle.

The mass of large fragments due to the predictions was to increase 17 times, but it increased only 8÷9 times (compare Figs.6.7 and 6.23).

Thus the results show that there cannot exist similarity parameters for such a complicated phenomena as breakup of a fuel tank and scaling of model tanks is a very difficult procedure. To apply the results of model experiments to the real fuel tank it is necessary to make use of general theoretical model of the type we described and not simple scaling parameters.

Part 7. Conclusions.

A theoretical model of a breakup of a fuel tank of space vehicle as a result of chemical explosion is worked out. A computer program for numerical simulation of the process is constructed. The test casesmatch the experimental results.

The results of numerical modelling show that the breakup process, the number, mass distributions and velocities of fragments differ greatly depending on the rate of energy release inside the tank for constant total TNT equiwalent of the explosion. The lowest rate of energy release is normal deflagration (or combustion), the medium rate - deflagration to detonation transition, the highest rate - detonation. It is proved theoretically that the dependence of the main breakup parameters on the rate of energy release is nonlinear and it is not monotonous. Thus it is necessary to take it into account and use the worked out numerical model to calculate the breakup parameters.

It is proved that there cannot exist any unique similarity criterion for the problem of breakup of a fuel tank as a result of chemical explosion. The breakup phenomenon is a combination of complicated processes of different physical nature. That is why there exist a lot of dimensionless similarity parameters and it is impossible to satisfy all of them without coming to a contradiction. Thus scaling of model experiments is impossible without making use of a profound theoretical and numerical model of the type described in this report.

Some of the important stages of the process can be the topics of further investigations. More complicated geometries of the shell will lead to new problems. The presence of weak zones in the shells of variable thickness can lead to a completely different scenario of breakup in cases of slow and intense loadings. The breakup scenario for different combinations of the variations of shell's thickness (shell nonuniformities) and rates of energy release is also to be investigated.

References.

For Part 1.

1.1. Preliminary Report No.1 "Investigation and Modelling of destruction of a space vehicle in course of chemical explosion". M.. 1994.

1.2. N.N.Smirnov, I.I.Panfilov, M.V.Tyurnikov and A.G.Berdynguin. Theoretical and experimental study of combustion to explosion transition in hydrocarbon-air mixtures. The 19th International Symposium on Space Technology and Science, 14-25 May 1994, Japan, 94-d-26.

1.3. Smirnov N.N., Tyurnikov M.V. A study of deflagration and detonation in Multiphase Hydrocarbon-Air Mixtures. Combustion and Flame. Elsevier Publishing Co., 1993.

For Part 2.

2.1. Vlasov O.E. Explosive waves. Moscow 1937.

2.2. Zeldovich,Ya.B., Kompaneets A.S. Detonation theory. Moscow, Gostehizdat, 1955.

2.3. Gas dynamics basis. Moscow, Izdatelstvo Inostrannoy Literature, 1963.

2.4. Sedov L.I. Similarity and Dimensionality Methods in Mechanics. Moscow, Nauka, 1981.

2.5. Smirnov N.N., Zverev I.N. Heterogeneous combustion. Moscow, Izdatelstvo MSU, 1992.

For Part 3.

3.1. Oppenheim, A.K., and Soloukhin R.I. Ann. Rev. Fluid Mech. 5: 31 (1973).

3.2. Salamandra, G.D. et al. Some methods of exploration of quick-going processes and their application to investigation of forming the detonation wave, Izdate.stvo Akademii Nauk SSSR, Moscow, 1960.

3.3. Soloukhin, R.I. Methods of measure and main results of experiments in shock tubes. Izdatelstvo Novosibirskogo Universiteta, Novosibirsk, 1969.

3.4. Clarke, J.F., and Riley, N. J.Fluid.Mech. 167 : 409-414 (1986)

3.5. Zeldovich, Ya.B., Librovich, V.B., Makhviladze, G.M., and Sivashinsky, G.I. Prikladnaya Mechanika i Technicheskaya Fizika, N 2: 76 (1970).

3.6. Gelfand, B.E., Makhviladze, G.M., Rogatykh, D.I., and Frolov, S.M. Spontaneous forming of explosive regimes of reaction in the regions with non-uniformities of temperature and concentration. Preprint N 358. Institut Problem Mekhaniki Akademii Nauk SSSR, Moscow, 1988.

3.7. Gelfand, B.E., Frolov, S.M., Polenov, A.N., and Tsyganov, S.A. Himicheskaya Fizika 5, N 9: 1277 (1986)

3.8. Clarke, J.F., Kassoy, D.R., and Riley, N. Proceeding of Royal Society A408: 129-148 (1986), London.

3.9. Smirnov, N.N., Demyanov, An.Yu., and Panfilov, I.I. Himicheskaya Fizika processov goreniya i vzryva. Detonatsya. Materialy IX Vsesoyuznogo Sympoziuma po Goreniyu i vzryvu. Izdatelstvo Akademii Nauk SSSR, Chernogolovka, 1989, p.52-56.

3.10. Urtiew, P.A. and Oppenheim, A.K, Experimental observations of the transition to detonation in an explosive gas, Proc. Roy. Soc., A295, 13, 1966.

3.11. Urtiew, P.A. and Oppenheim, A.K. Transverse flame-shock interactions in an explosive gas, Proc. Roy. Soc., A304, 379, 1968.

3.12. Laffite P. Comp. Rend. Acad. Sci. Paris 1923, V.176, P.1392.

3.13. Schelkin K.I., Troshin Ya. K. Combustion gasdynamics. Moscow: Izdatelstvo AN SSSR, 1963.

3.14. Hitrin L.N. Combustion and explosion physics. Moscow, Izdatelsvo MGU, 1957.

3.15. Zeldovich Ya. B., Barenblatt G.I., Librovich V.B., Machviladze G.M. Mathematical combustion theory. Moscow.

3.16. Zeldovich Ya.B. Chemical physics and hydrodynamics. Moscow. Nauka. 1984.

For Part 4.

4.1. Fragmentation experiments for the Evolution of the Small Size Debris Population. //Proc. of the First European Conf. on Space Debris. Darmstadt. 1993. P.275-280 (ESA SD-01).

4.2. Kiselev A.B. The Simplest Mathematical Model of Spacecraft Failure in Explosion.// Vestnik Moskovskogo Universiteta. Seriya Mathematika i Mechanika. 1993. Vol.48. No.4. p.49-53 (in Russian).

4.3. Kiselev A.B. Mathematical Modelling of Fragmentation of Thin Shells in Explosion.// Proc. of the Int. IMACS Symposium on Mathematical Modelling. Vol.5. Vienna. 1994. p.882-884.

4.4. Kiselev A.B., Yumashev M.V. On Dynamic Failure Criterion for a Thermoelastoplastic Medium.// Vestnik Moskovskogo Universiteta. Seriya Mathematika i Mechanika. 1990. vol.45. No.4, pp.38-43 (in Russian).

4.5. Ivanov A.G. The Function of Inertial and Elastic Forces under Dynamic Fracture in Plastic Region.// Dokl. Akad. Nauk SSSR. 1991. Vol.321. No.1. pp.28-32 (in Russian).

4.6. Perzina P. The Constitutive Equations for Rate Sensitive Plastic Materials.// Quart. Appl. Mech., 1993. vol.20. No.3. pp.321-332.

4.7. Odintsov V.A. The Bimodal Distribution of Cylindrical Fragments.// Fizika Goreniya i Vzryva. 1991, No.5. pp.118-122 (in Russian).

4.8. Odintsov V.A. The Two-dimensional Distribution of Cylindrical Fragments on Mass and Form Characteristic.// Fizika Goreniya i Vzryva. 1993. No.1. pp.123-133 (in Russian).

4.9. Wilkins M.L. Modelling the Behaviour of Materials.// Struct. Impact and Crashworth: Proc. Int. Conf., V.2. L.; N.Y., 1984. pp.243-277.

4.10. Kanel'G.I., Razorenov S.V., Fortov V.E. Break-off strength of metals in a wide range of amplitudes of impact loads.// Dokl. Akad. Nauk SSSR. 1987. Vol.294. No.2. pp.350-352 (in Russian).

For Part 5.

5.1. Samarsky A.A., Popov Yu.P. Differential schemes for gas dynamics. Moscow, "Nauka". 1975. 352 pages (in Russian).

5.2. Bakhvalov N.S., Zhidkov N.P., Kobelkov D.M. Numerical methods. Moscow, "Nauka". 1987. 600 pages (in Russian).

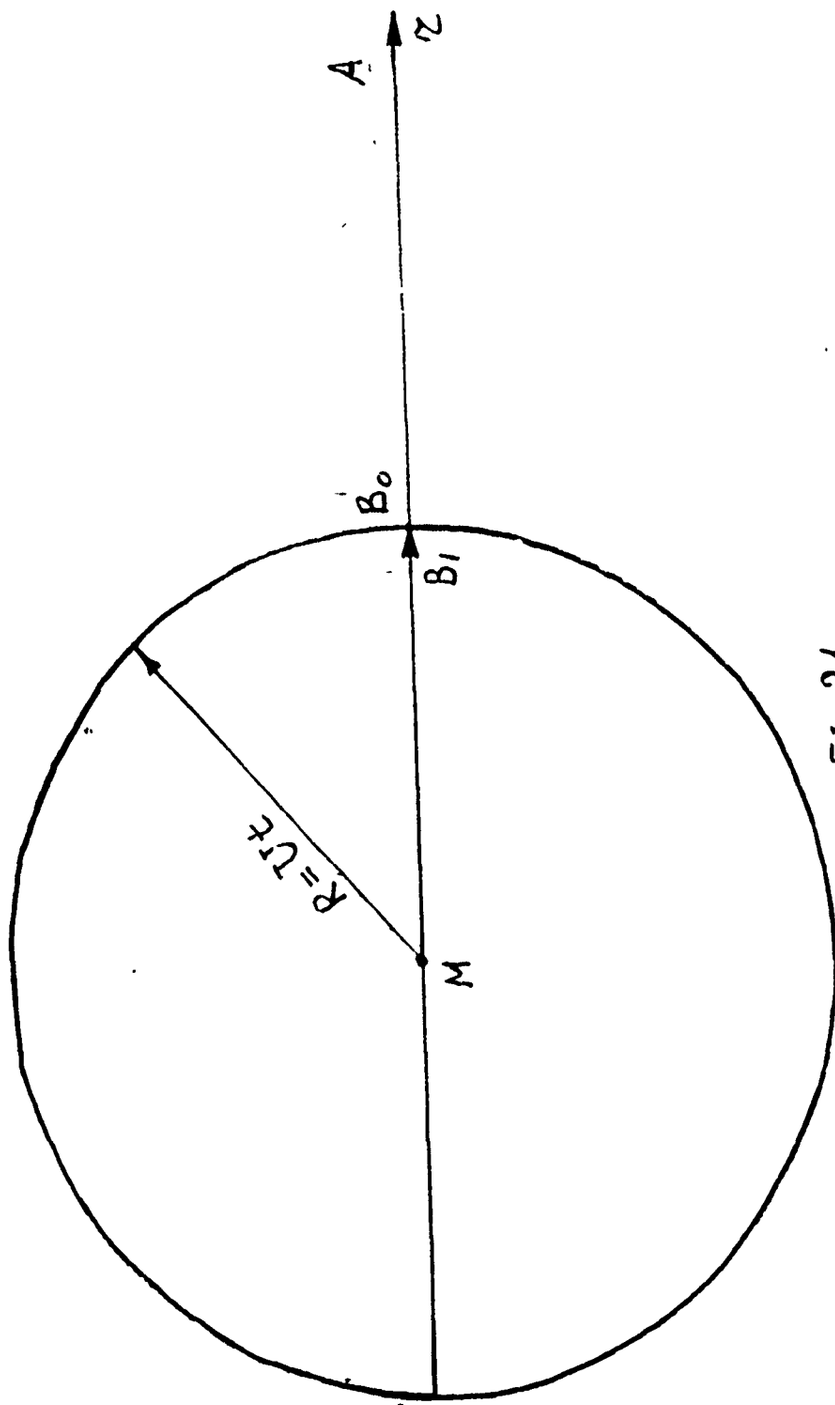

Fig.21

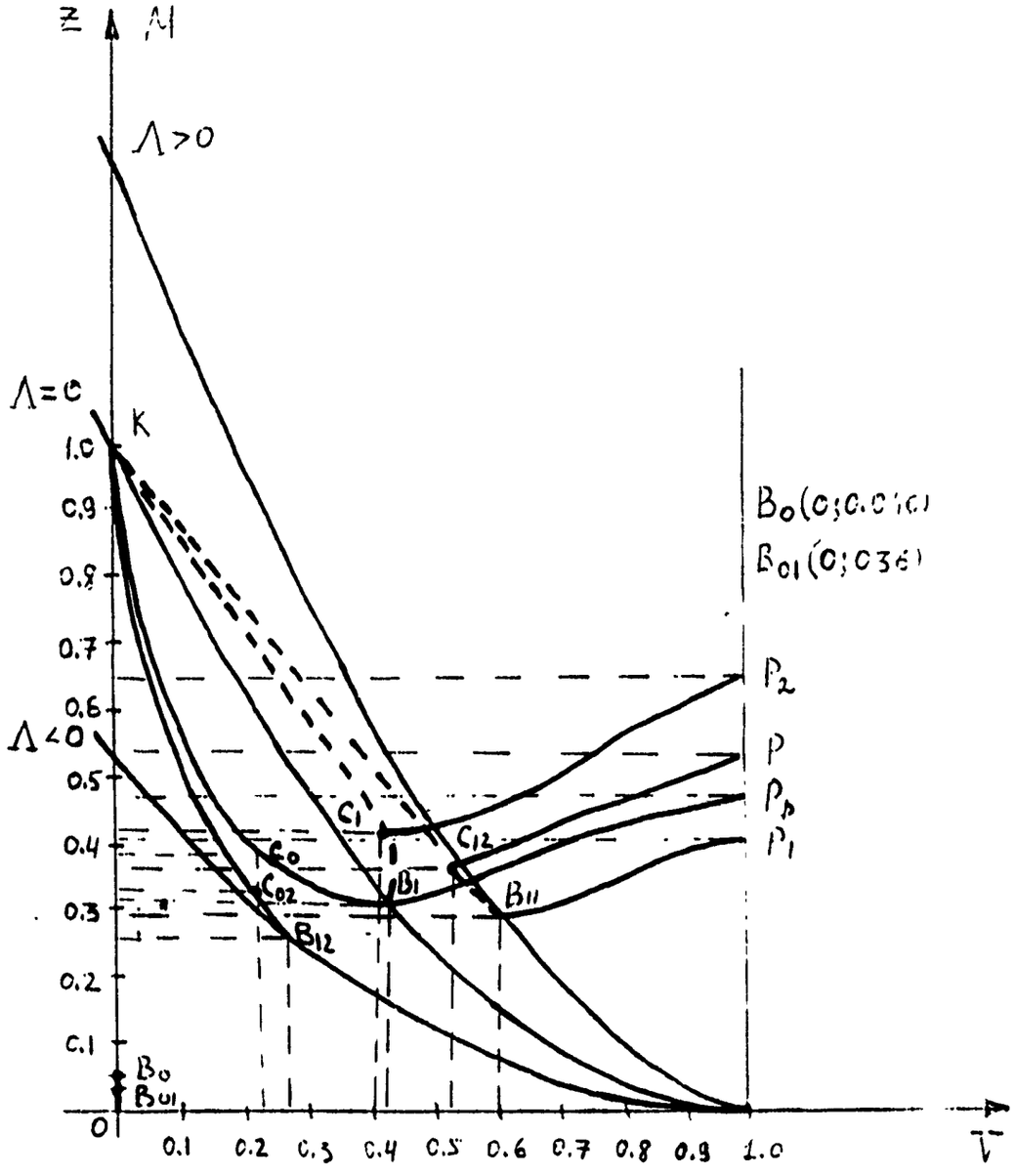
Z
M
Λ>0
Λ=0
K
1.0
0.9
0.8
0.7
0.6
Λ<0
0.5
0.4
0.3
0.2
0.1
0
B₀
B₀₁
B₀(0;0.01;0)
B₀₁(0;0.36)
P₂
P
P₀
P₁
C₁
C₁₂
C₀
C₀₂
B₁
B₁₁
B₁₂
0.1
0.2
0.3
0.4
0.5
0.6
0.7
0.8
0.9
1.0
V

Fig. 2.2.

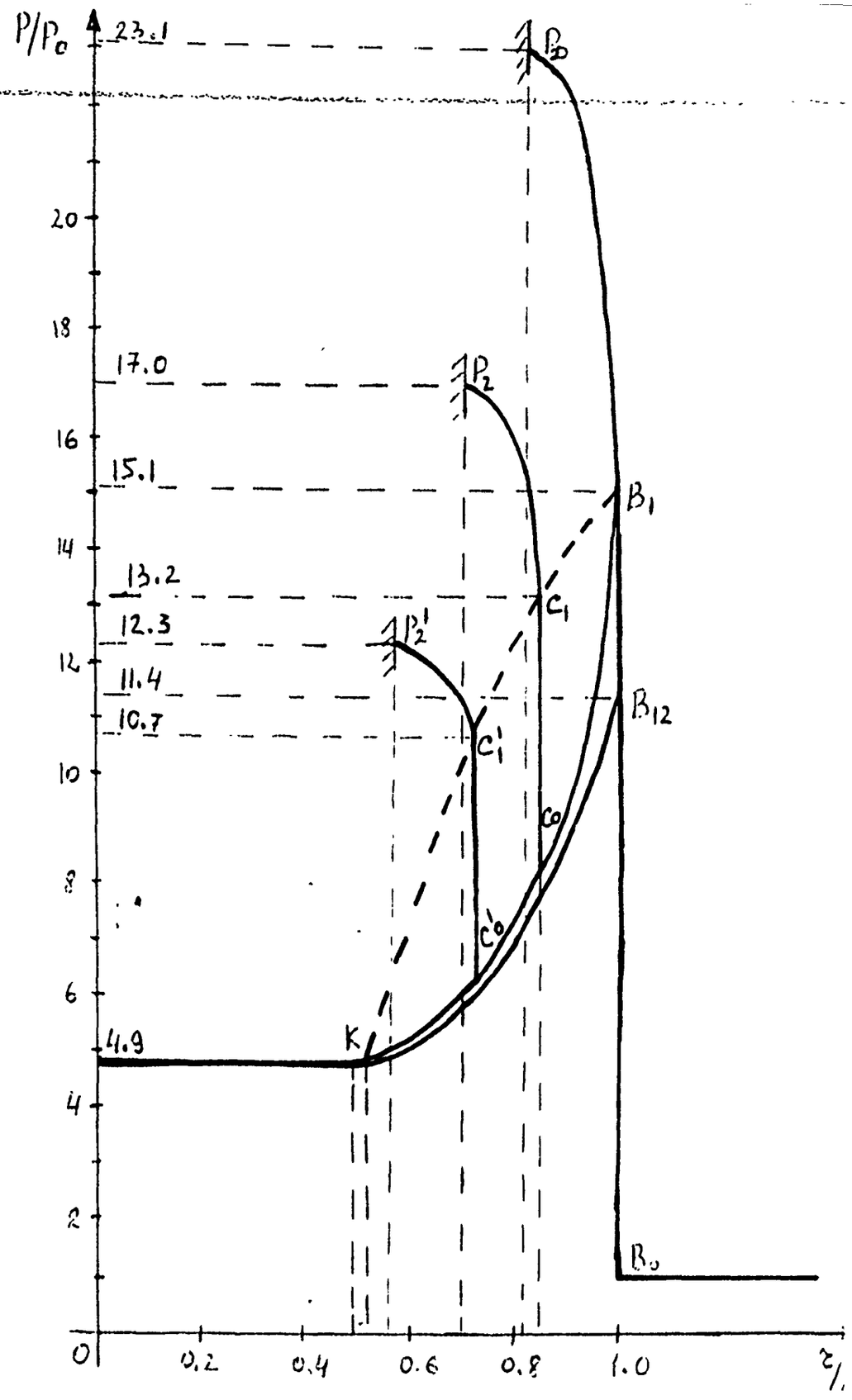
P/P₀
23.1
20
18
17.0
16
15.1
14
13.2
12.3
12
11.4
10.7
10
8
6
4.9
4
2
0
0.2
0.4
0.6
0.8
1.0
z/
P₂
B₁
C₁
P₂'
B₁₂
C₁'
C₀
C₀'
K
B₀

Fig2.3.

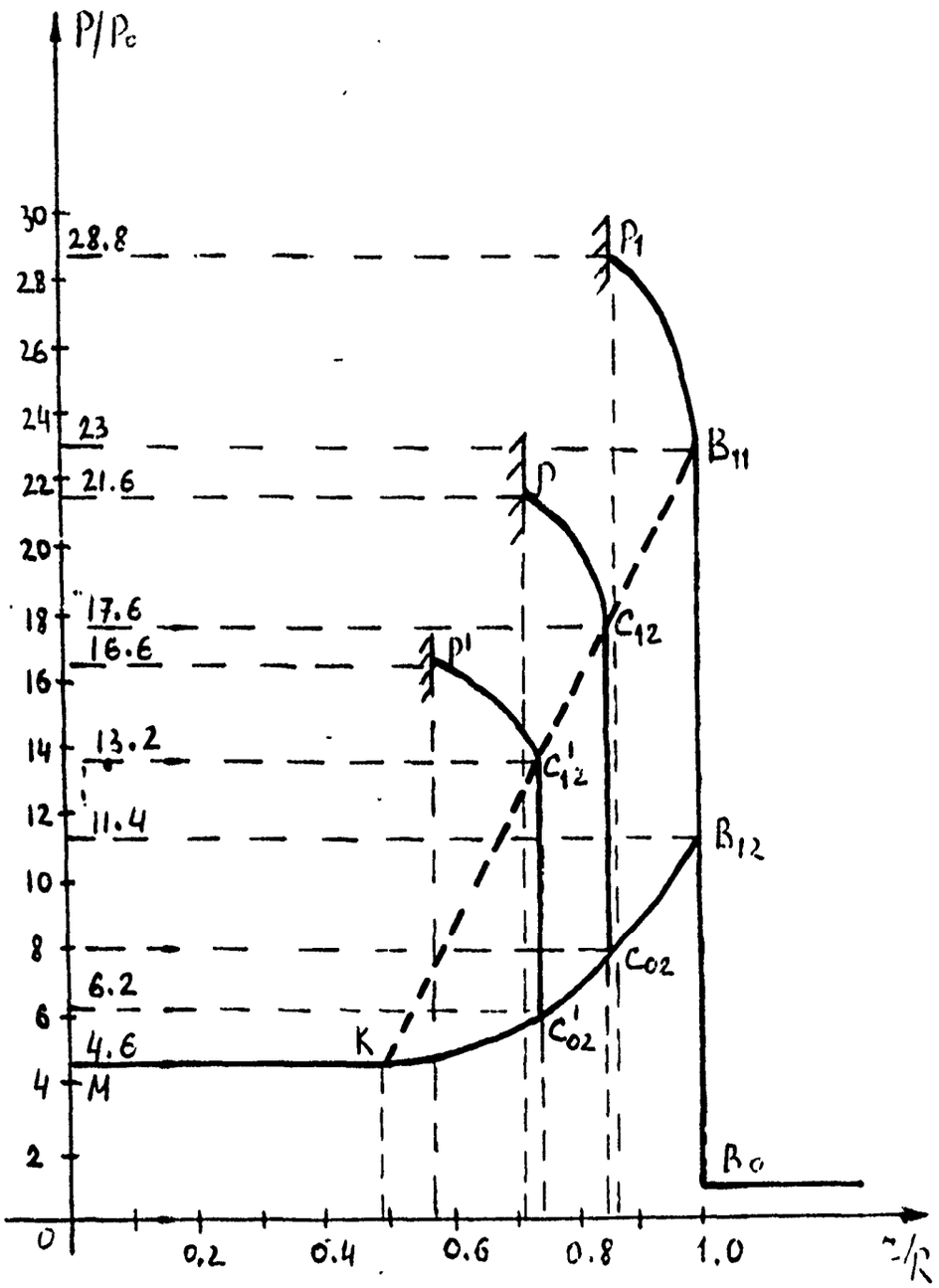
P/Pc
30
28.8
28
26
24
23
22
21.6
20
18
17.6
16.6
16
14
13.2
12
11.4
10
8
6.2
6
4.6
4
M
2
0
0,2
0.4
0.6
0.8
1.0
z/R
P1
B11
D
C12
P'
C'12
B12
C02
C'02
K
B0

Fig.2.4.

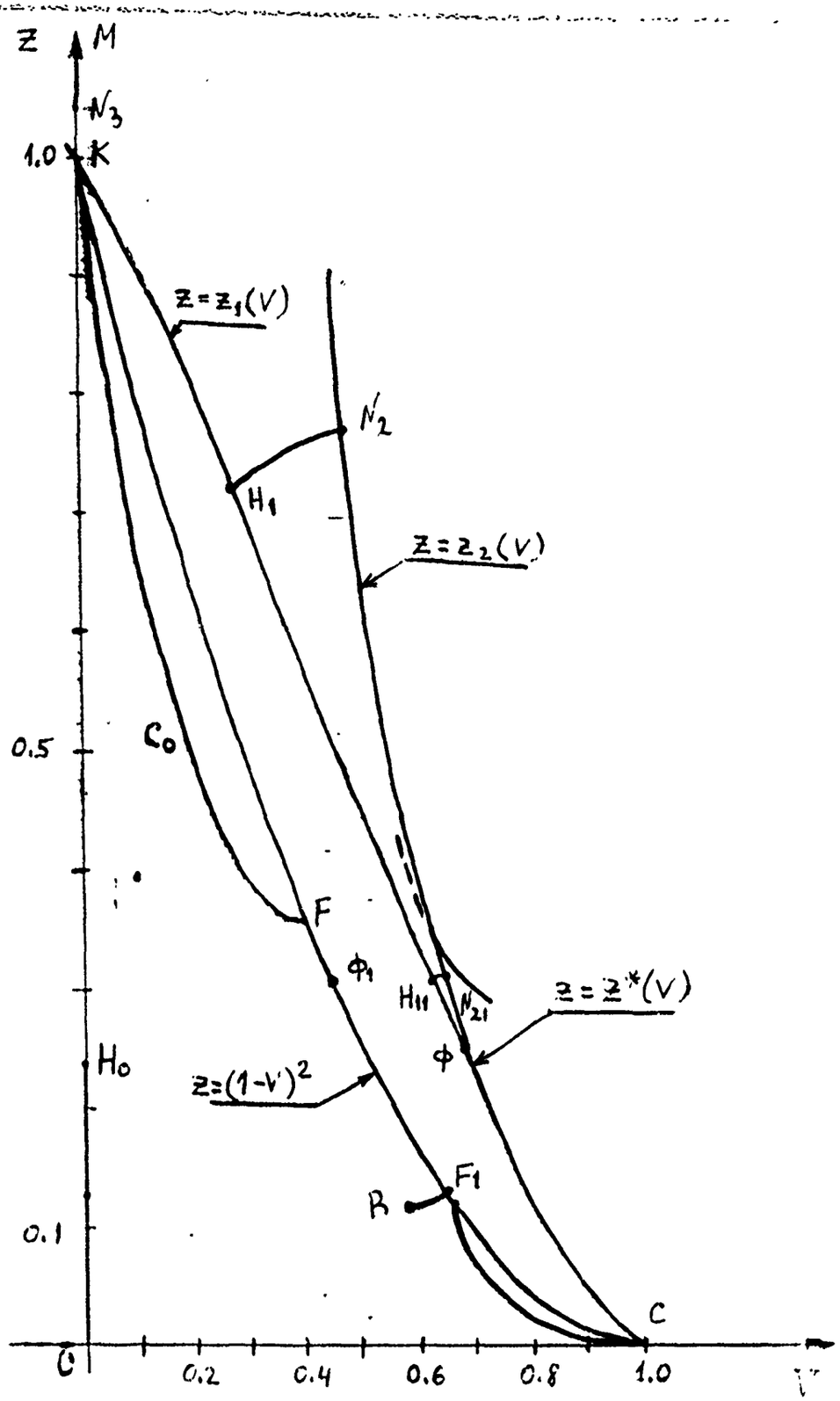
z
M
N3
1.0
K
z = z1(V)
N2
H1
z = z2(V)
0.5
C0
F
Φ1
H11
N21
z = z*(V)
Φ
H0
z=(1-v')2
F1
B
0.1
C
0
0.2
0.4
0.6
0.8
1.0
V

Fig.2.5.

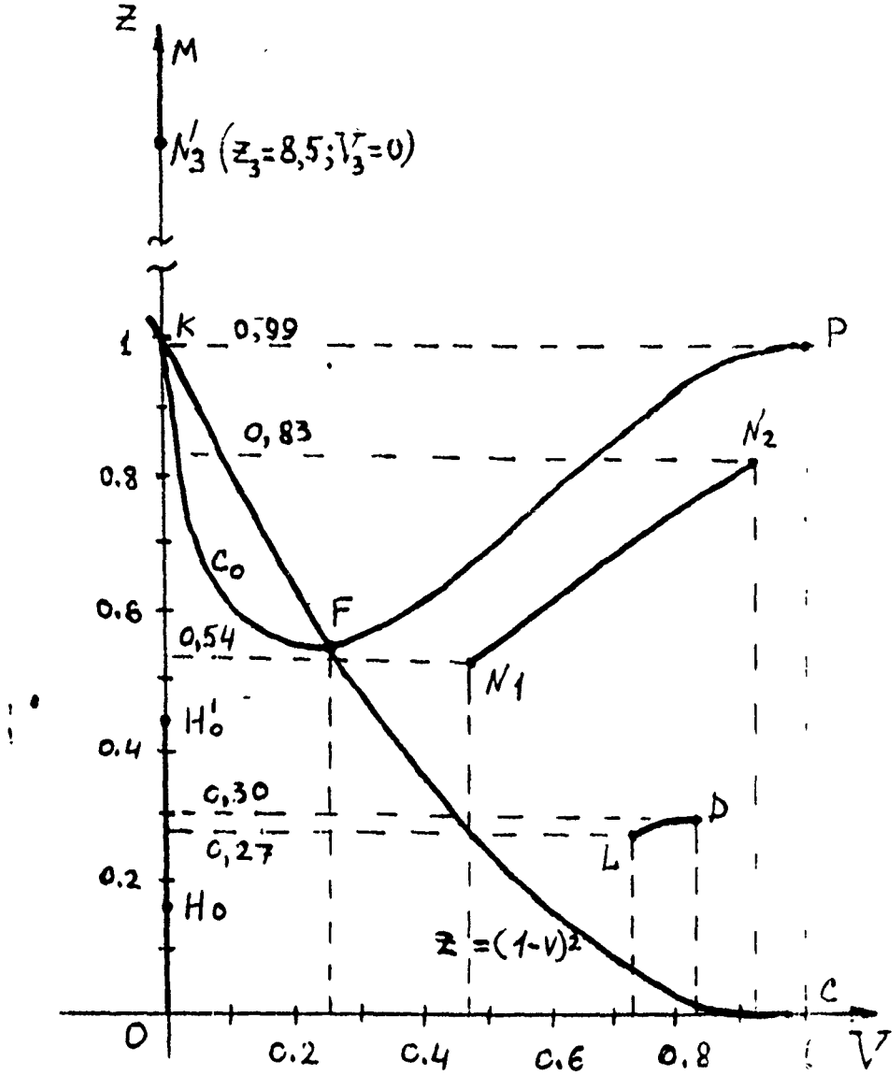
Z
M
N_3' (Z_3=8,5; $\bar{V}_3$=0)
1
K
0,99
P
0,83
N_2
0.8
C_0
0.6
F
0,54
N_1
H_0'
0.4
0,30
0,27
D
L
0.2
H_0
$Z=(1-V)^2$
C
O
0.2
0.4
0.6
0.8
V

Fig.2.6.

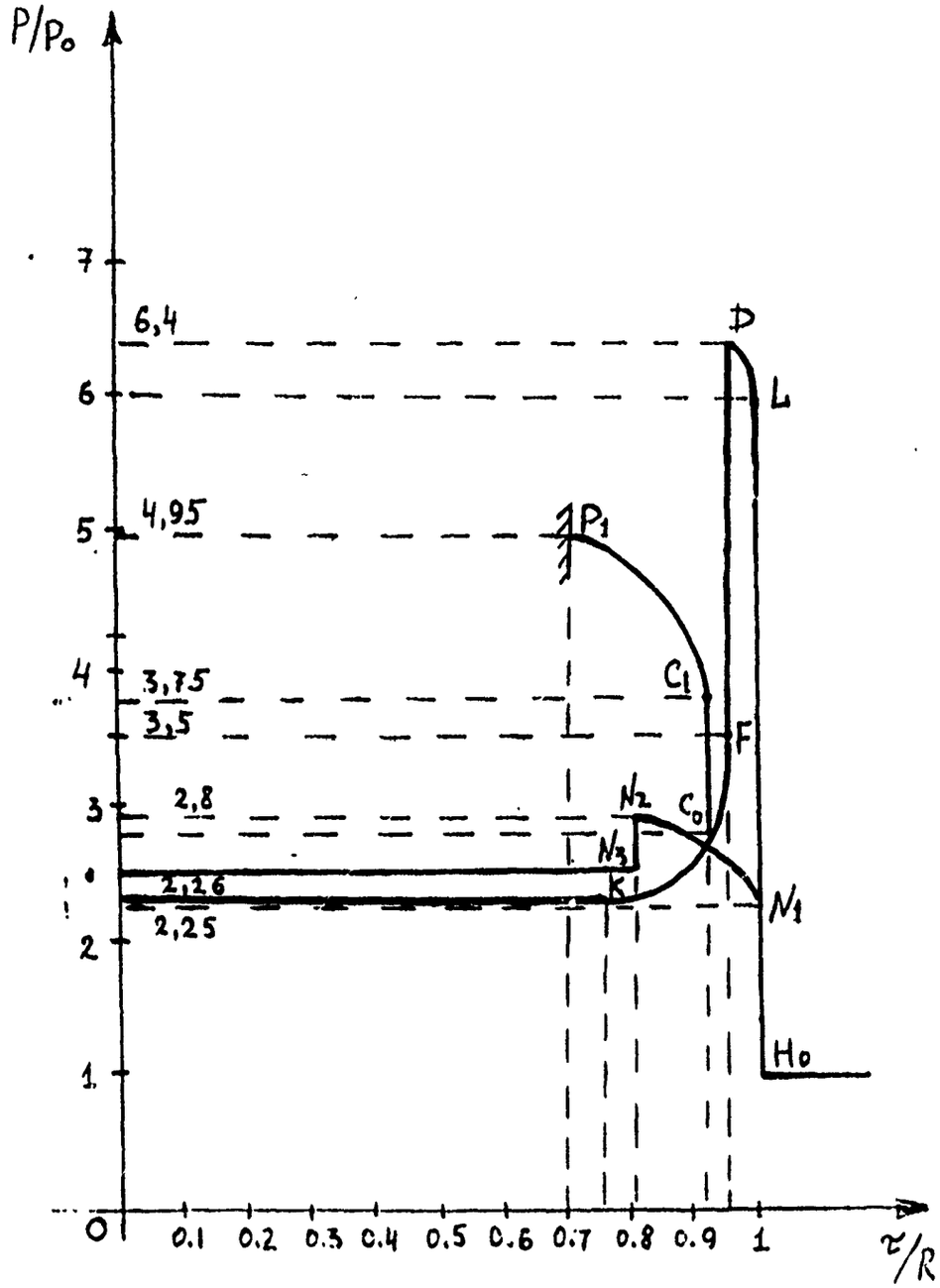
P/P₀
7
6,4
6
4,95
5
4
3,75
3,5
3
2,8
2,126
2,25
2
1
0
0.1
0.2
0.3
0.4
0.5
0.6
0.7
0.8
0.9
1
r/R
D
L
P₁
C₁
F
N₂
C₀
N₃
K
N₁
H₀

Fig.2.7.

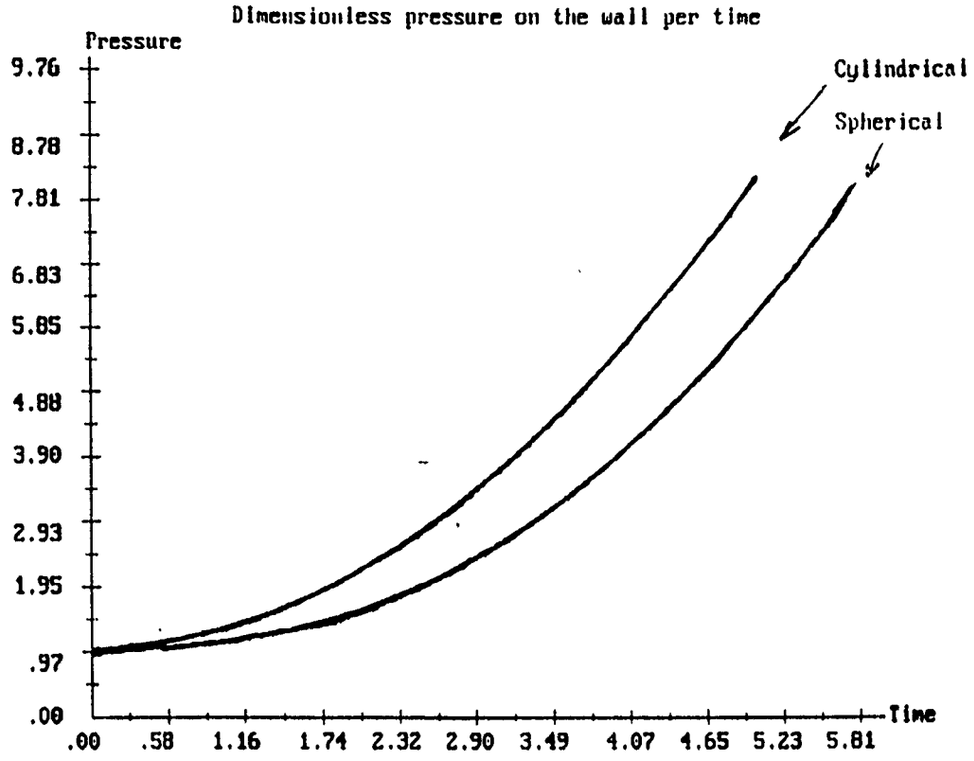
Dimensionless pressure on the wall per time
Pressure
9.76
8.78
7.81
6.83
5.85
4.88
3.90
2.93
1.95
.97
.00
Cylindrical
Spherical
.00
.58
1.16
1.74
2.32
2.90
3.49
4.07
4.65
5.23
5.81
Time

Fig. 3.1.

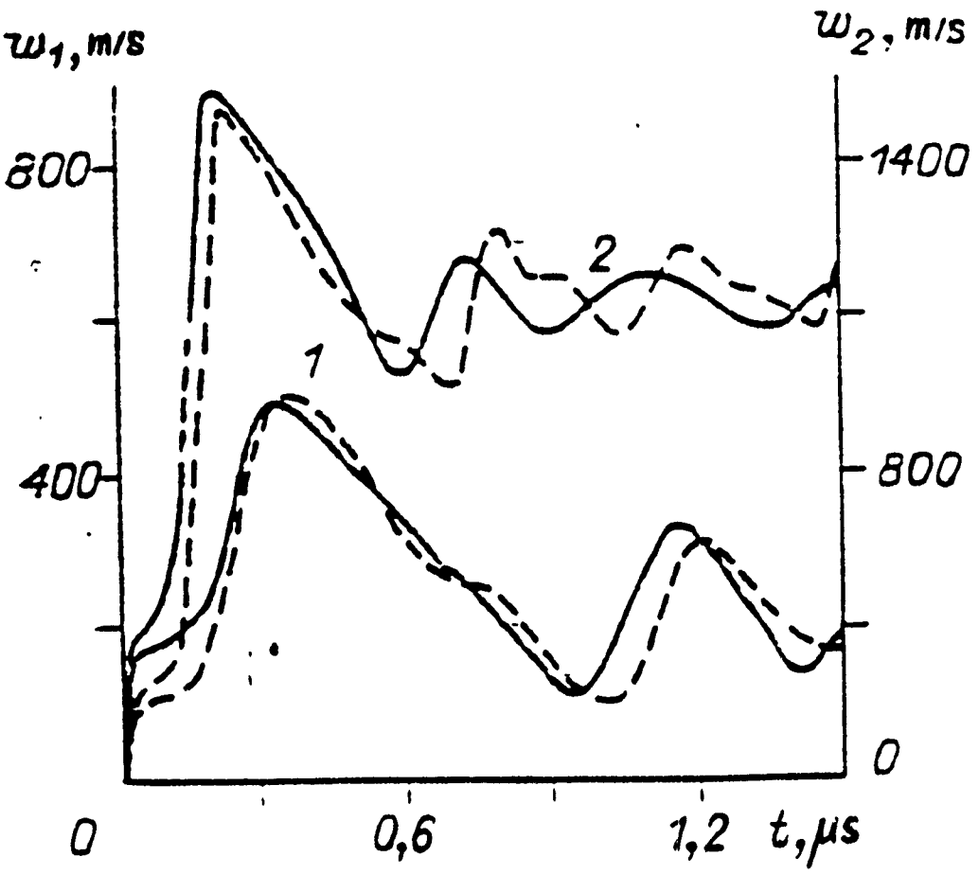

Fig. 4.1.

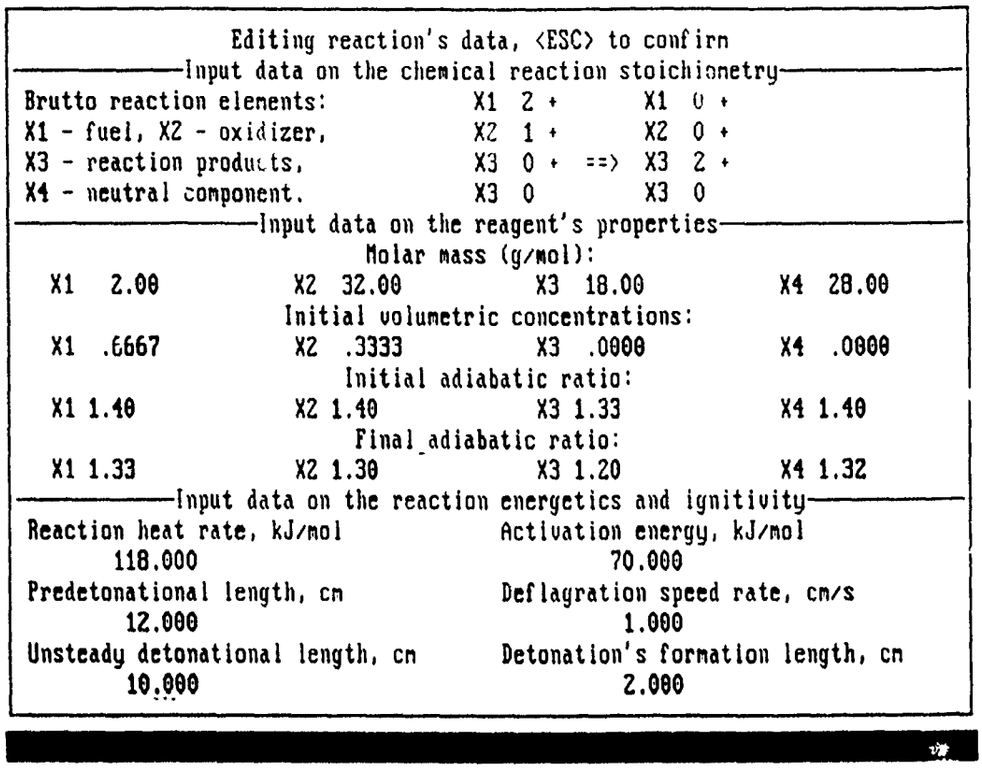
Editing reaction's data, <ESC> to confirm
Input data on the chemical reaction stoichiometry
Brutto reaction elements:
X1 - fuel, X2 - oxidizer,
X3 - reaction products,
X4 - neutral component.
X1 2 + X1 0 +
X2 1 + X2 0 +
X3 0 + ==> X3 2 +
X3 0 X3 0
Input data on the reagent's properties
Molar mass (g/mol):
X1 2.00 X2 32.00 X3 18.00 X4 28.00
Initial volumetric concentrations:
X1 .6667 X2 .3333 X3 .0000 X4 .0000
Initial adiabatic ratio:
X1 1.40 X2 1.40 X3 1.33 X4 1.40
Final adiabatic ratio:
X1 1.33 X2 1.30 X3 1.20 X4 1.32
Input data on the reaction energetics and ignitivity
Reaction heat rate, kJ/mol
118.000
Activation energy, kJ/mol
70.000
Predetonational length, cm
12.000
Deflagration speed rate, cm/s
1.000
Unsteady detonational length, cm
10.000
Detonation's formation length, cm
2.000

Fig. 6. 1.

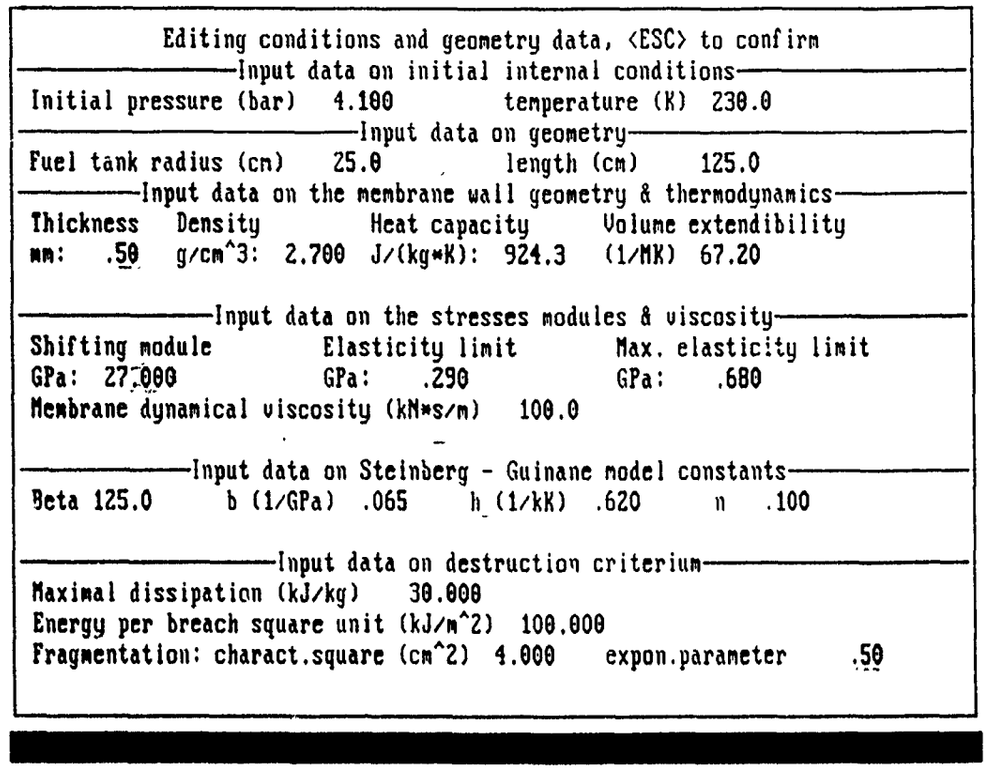
Editing conditions and geometry data, <ESC> to confirm
Input data on initial internal conditions
Initial pressure (bar) 4.100 temperature (K) 230.0
Input data on geometry
Fuel tank radius (cm) 25.0 length (cm) 125.0
Input data on the membrane wall geometry & thermodynamics
Thickness Density Heat capacity Volume extendibility
mm: .50 g/cm^3: 2.700 J/(kg*K): 924.3 (1/MK) 67.20
Input data on the stresses modules & viscosity
Shifting module Elasticity limit Max. elasticity limit
GPa: 27.000 GPa: .290 GPa: .680
Membrane dynamical viscosity (kN*s/m) 100.0
Input data on Steinberg - Guinane model constants
Beta 125.0 b (1/GPa) .065 h (1/kK) .620 n .100
Input data on destruction criterium
Maximal dissipation (kJ/kg) 30.000
Energy per breach square unit (kJ/m^2) 100.000
Fragmentation: charact.square (cm^2) 4.000 expon.parameter .50

Fig. 6.2

Internal process results

Concentrations of reagents

	X1	X2	X3	X4
Volumetric initial concentration	.66670	.33330	.00000	.00000
Mass initial concentrations	.11112	.88887	.00000	.00000
Volumetric final concentrations	.00014	.00000	.99985	.00000
Mass final concentrations	.00001	.00000	.99998	.00000

Molar masses of reagent mixtures, g/mol

Initial: 11.9 Final: 17.9

Specific heats of mixture at constant volume, J/(kg*K)

Initial: 1731.3 Final: 2308.5

Adiabatic ratii of mixture

Initial: 1.400 Final: 1.200

Reaction's heat release

Release per mol (kJ/mol): 117.988 Release per mass (kJ/kg): 9833.169

Equilibrium final conditions

Pressure (bar): 52.673 Temperature (K): 4432.0

Type of the process inside the fuel tank

Normal detonation

Press any key to continue

Fig 6.3

Internal process results (continued)

Time-pressure characteristics of the process

	Cylinder	Sphere
Pressure (bar):		
Initial	4.100	4.100
Before shock	4.100	4.100
After shock	194.385	194.385
After reaction zone	93.064	93.064
After shock's reflection	1376.750	1376.750
After reaction zone's reflection	229.173	229.173
Final	52.673	52.673
Detonation's wave velocity (km/s)	3.015	3.015
Time intervals (ms):		
Ignition -- detonation origin	1028.829	669.482
Detonation origin -- reflection	.043	.043
Reaction zone near the wall duration	.009	.009
Relaxation time	.082	.082
Active pressure increase duration	.092	.092

Press any key to continue

Fig 6.4

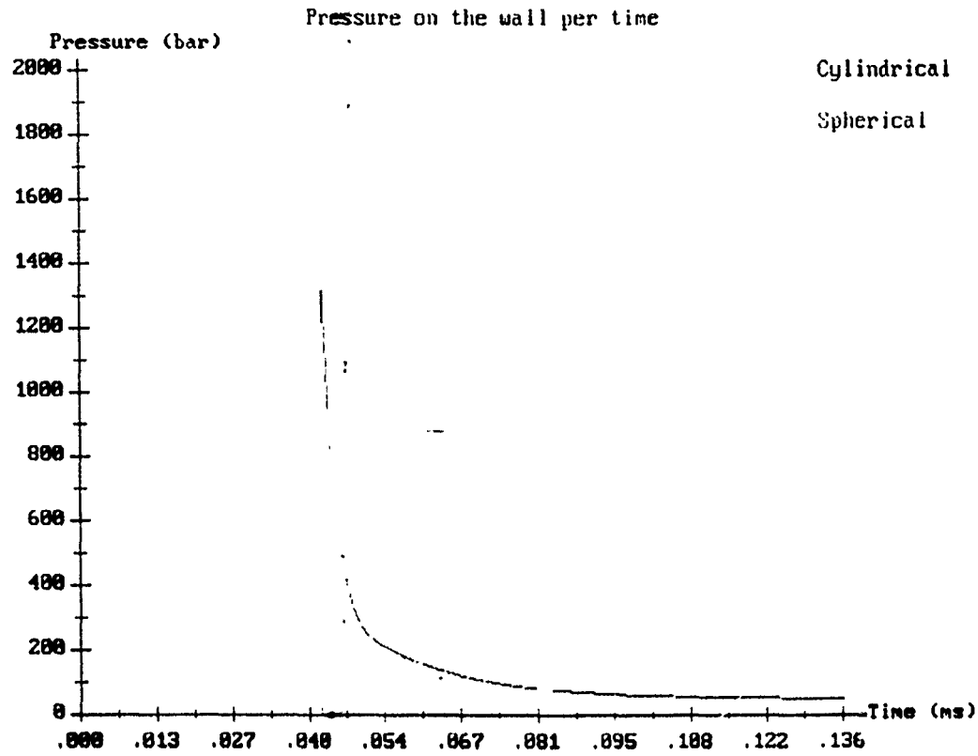
Pressure on the wall per time
Pressure (bar)
2000
1800
1600
1400
1200
1000
800
600
400
200
0
Cylindrical
Spherical
Time (ms)
.000
.013
.027
.040
.054
.067
.081
.095
.108
.122
.136

Fig. 6.5.

Tank wall breakup by internal pressure increase results

Loading on the wall

	Cylindrical	Spherical
Impulse per square (bar*s)	.011871	.011871
Dissipation per mass (kJ/kg)	36.5492	36.5492
Elastic energy per mass (kJ/kg)	78.7556	78.7556
Final density (g/cm^3)	1.9131	1.9131
Final velocity (m/s)	973.4301	973.4301
Loading time (ms):	.2001	.2001
Wall destruction time (ms):	.1232	.1232
Fragmentation occurs:	Yes	Yes

Press any key to continue

Fig 6.6

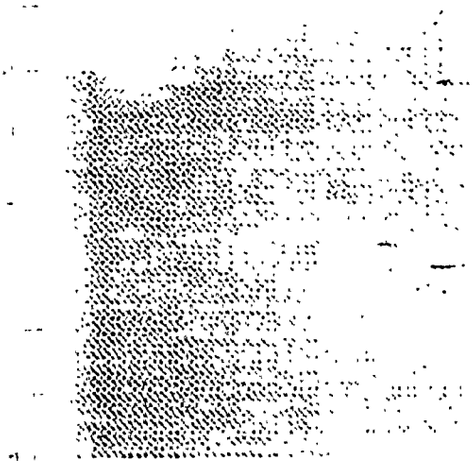

Fig. 6.7

On-Ground Fragmentation Test Results

Test Conditions: ESOC-1/2/3 → Δp = 3.1/2.9/4.1 bar, T = +20/-45/-45°C

	ESOC 1	*ESOC 2*	*ESOC 3*
TNT-equivalent	1.33 kg	1.72 kg	2.13 kg
number of fragments	634	1302	1762
recovered wall mass	99.5 %	98.7 %	98.2 %
assigned particles	97.9 %	95.7 %	90.8 %
maximum of N(m) distribution	0.73 g	0.24 g	0.24 g
average fragment mass	0.276 g	0.137 g	0.104 g
maximum fragments/bin	88	174	240

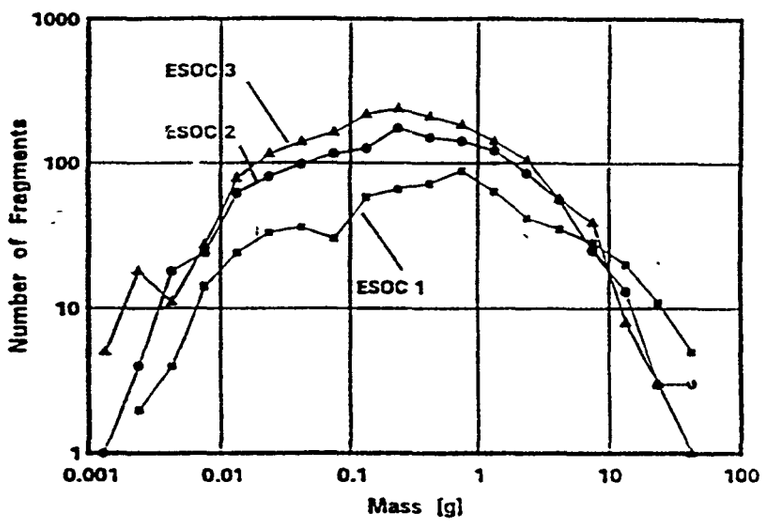

Fragmentation Statistics **Mass Distributions**

- **Conclusion: the Battelle test series, yielded valuable data on mass spectra and incremental velocities for different explosive inventories and test conditions; the tests do, however, fail to explain small-size debris observed on orbit**

Fig. 6.8.

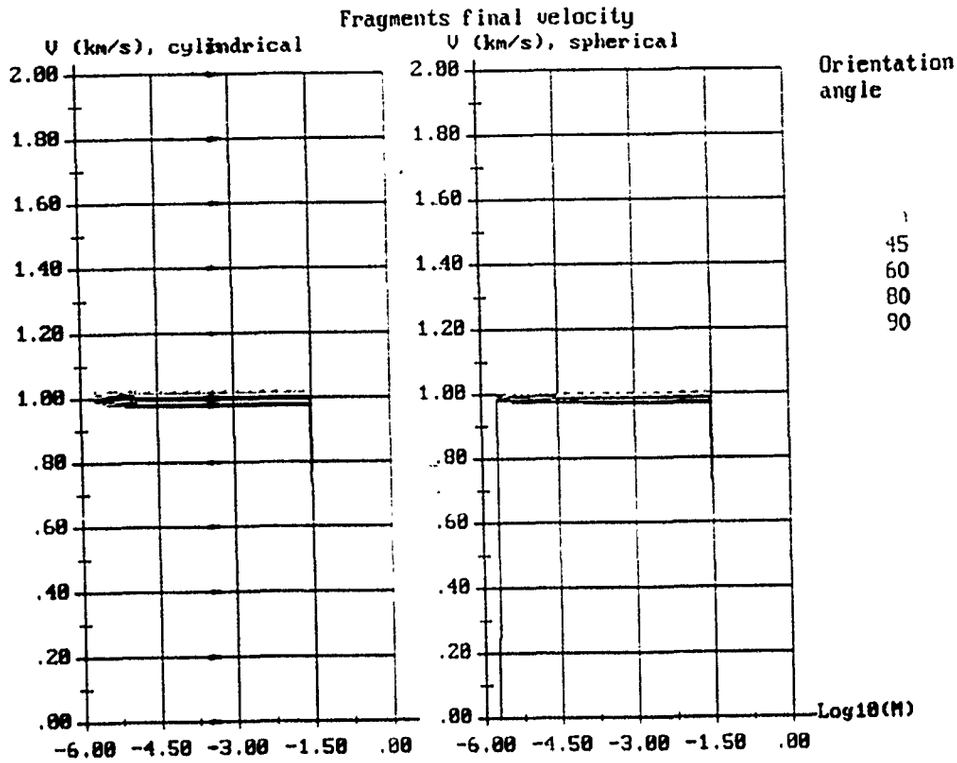
Fragments final velocity
V (km/s), cylindrical
V (km/s), spherical
Orientation angle
45
60
80
90
2.00
1.80
1.60
1.40
1.20
1.00
.80
.60
.40
.20
.00
-6.00 -4.50 -3.00 -1.50 .00
Log10(M)

Fig. 6.9.

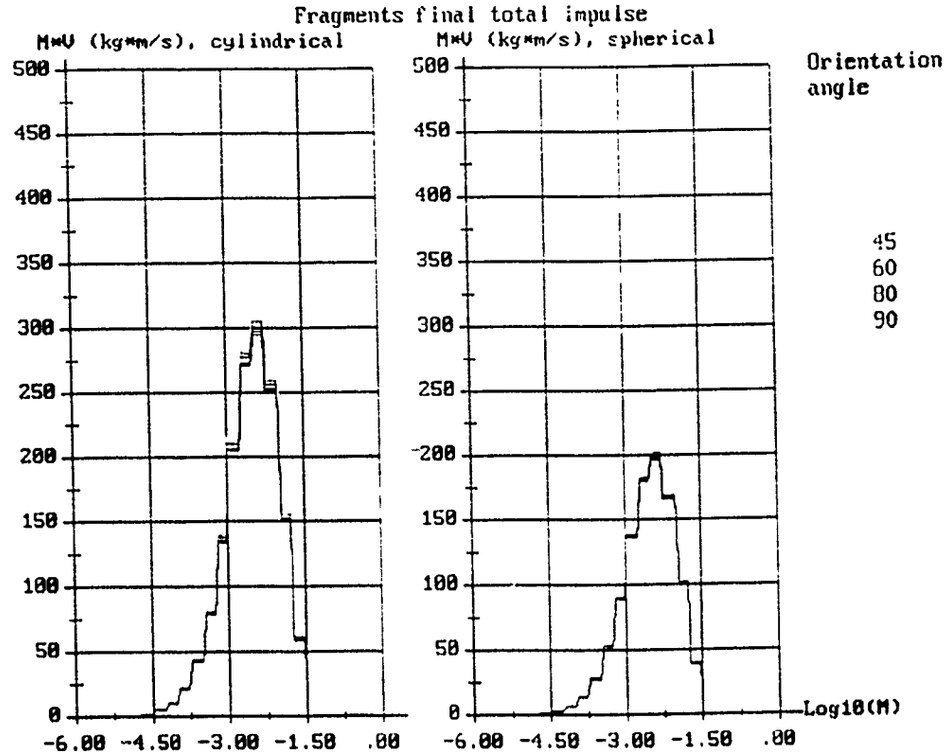
Fragments final total impulse
M*V (kg*m/s), cylindrical
M*V (kg*m/s), spherical
Orientation angle
500
450
400
350
300
250
200
150
100
50
0
-6.00 -4.50 -3.00 -1.50 .00
45
60
80
90
Log10(M)

Fig 6.10.

Internal process results (continued)

Time-pressure characteristics of the process

	Cylinder	Sphere
Pressure (bar):		
Initial	4.100	4.100
Before shock	4.100	4.100
After shock	4.100	4.100
After reaction zone	4.100	4.100
After shock's reflection	4.100	4.100
After reaction zone's reflection	4.100	4.100
Final	52.673	52.673
Detonation's wave velocity (km/s)	.000	.000
Time intervals (ms):		
Deflagration process duration	7017.515	5296.636

Press any key to continue

Fig 6.11

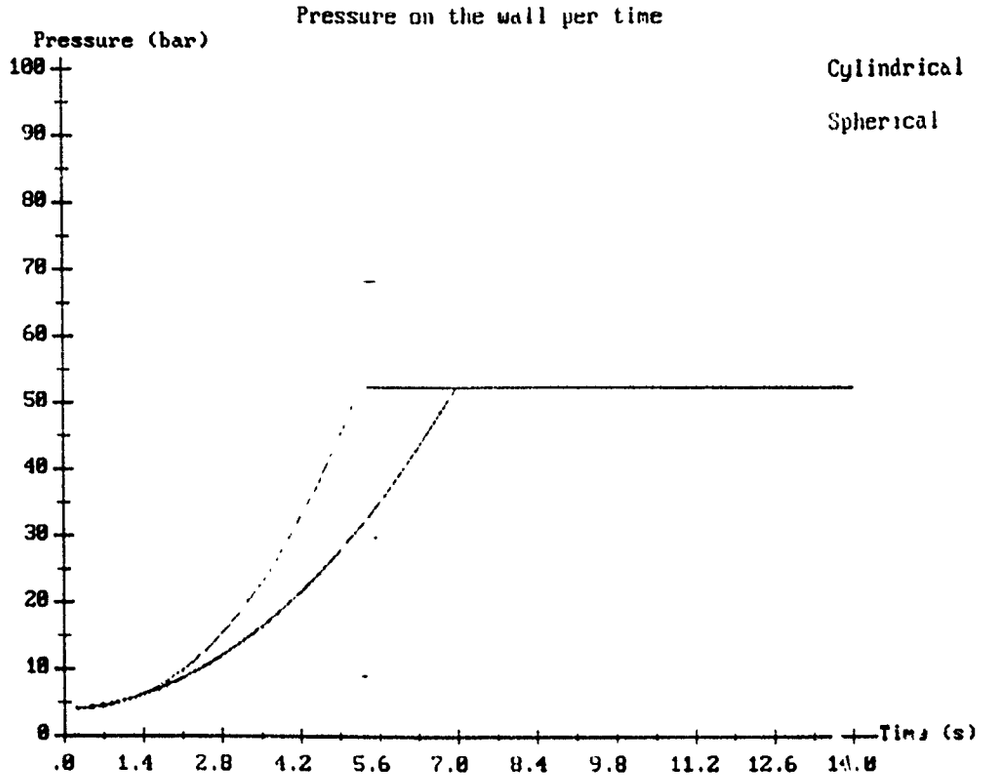
Pressure on the wall per time
Pressure (bar)
100
90
80
70
60
50
40
30
20
10
0
Cylindrical
Spherical
.0
1.4
2.8
4.2
5.6
7.0
8.4
9.8
11.2
12.6
Time (s)

Fig 6.1a.

Tank wall breakup by internal pressure increase results

Loading on the wall

	Cylindrical	Spherical
Impulse per square (bar*s)	.010069	.010069
Dissipation per mass (kJ/kg)	37.4761	37.4761
Elastic energy per mass (kJ/kg)	78.5099	78.5099
Final density (g/cm^3)	1.7791	1.7791
Final velocity (m/s)	877.4780	877.4780
Loading time (ms):	.2871	.2871
Wall destruction time (ms):	.1911	.1911
Fragmentation occurs:	Yes	Yes

Press any key to continue

Fig. 13.

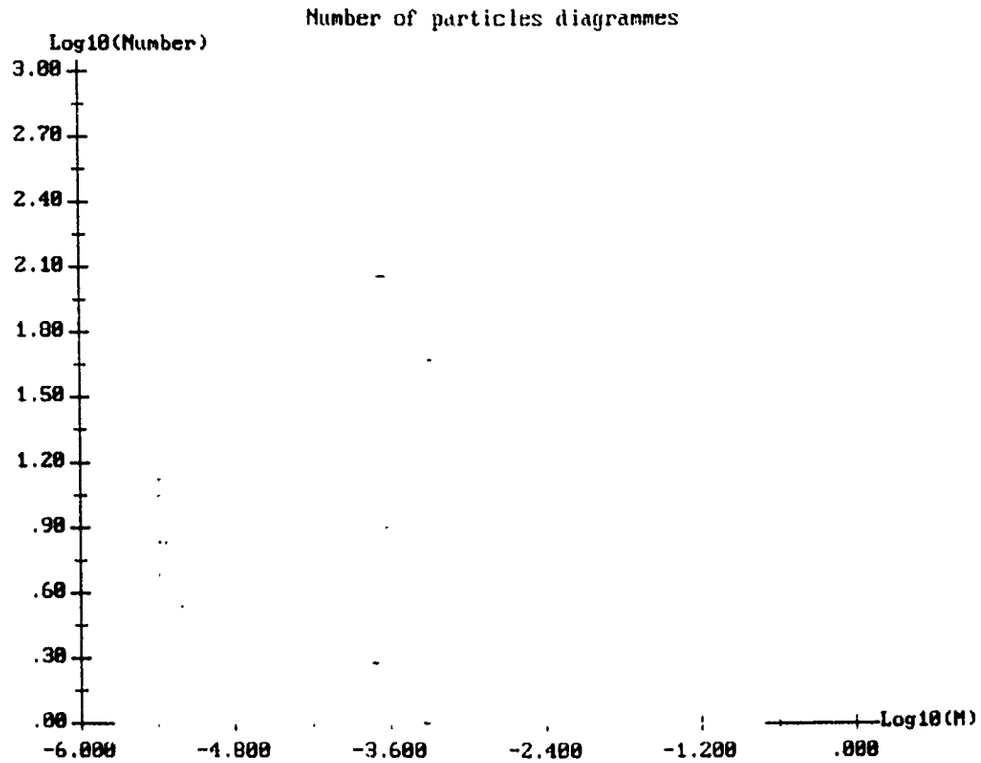
Number of particles diagrammes
Log10(Number)
3.00
2.70
2.40
2.10
1.80
1.50
1.20
.90
.60
.30
.00
Log10(M)
-6.000
-4.800
-3.600
-2.400
-1.200
.000

Fig 6.17

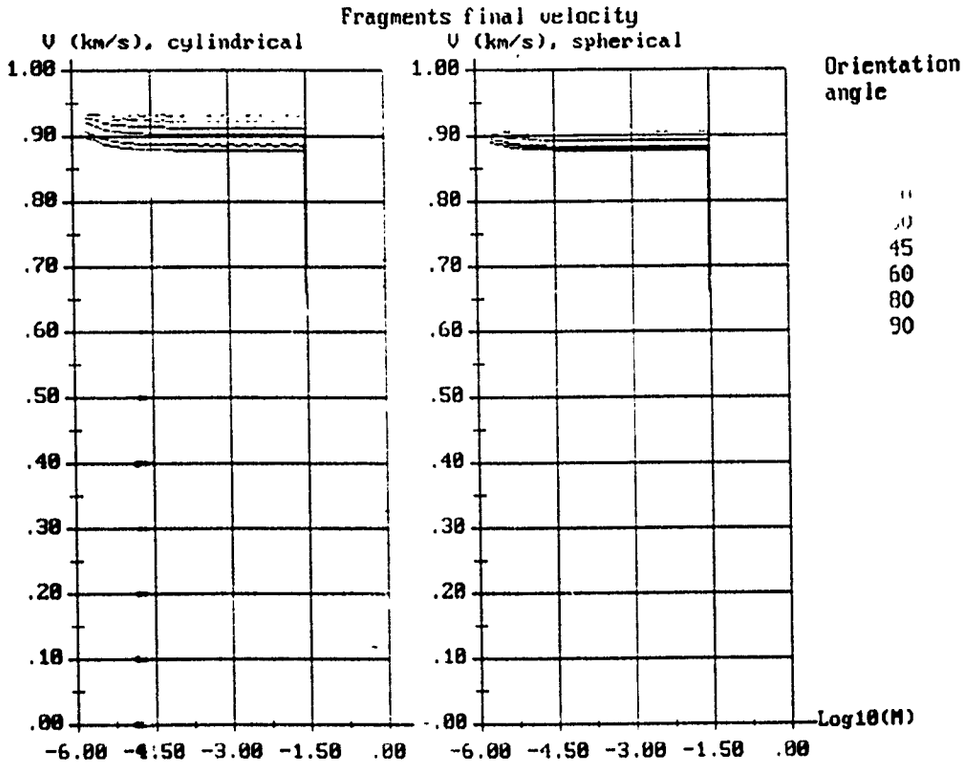
Fragments final velocity
V (km/s), cylindrical
V (km/s), spherical
Orientation angle
45
60
80
90
1.00
.90
.80
.70
.60
.50
.40
.30
.20
.10
.00
-6.00 -4.50 -3.00 -1.50 .00
Log10(M)

Fig. 6.15.

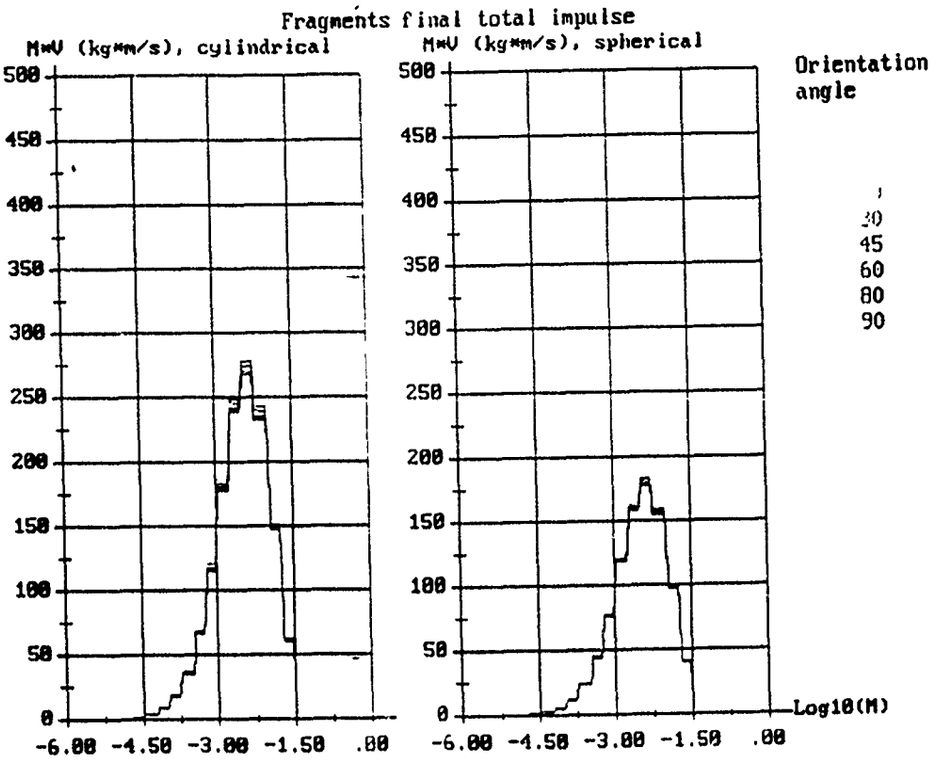
Fragments final total impulse
M*V (kg*m/s), cylindrical
M*V (kg*m/s), spherical
Orientation angle
500
450
400
350
300
250
200
150
100
50
0
-6.00 -4.50 -3.00 -1.50 .00
30
45
60
80
90
Log10(M)

Fig. 6.16.

Internal process results (continued)

Time-pressure characteristics of the process

	Cylinder	Sphere
Pressure (bar):		
Initial	4.100	4.100
Before shock	22.194	17.186
After shock	667.276	553.164
After reaction zone	323.792	267.774
After shock's reflection	4431.610	3715.500
After reaction zone's reflection	780.481	647.921
Final	52.673	52.673
Detonation's wave velocity (km/s)	3.059	3.051
Time intervals (ms):		
Ignition -- detonation origin	4271.789	2994.654
Detonation origin -- reflection	.006	.006
Reaction zone near the wall duration	.015	.014
Relaxation time	.081	.081
Active pressure increase duration	.097	.096

Press any key to continue

Fig. 6.17

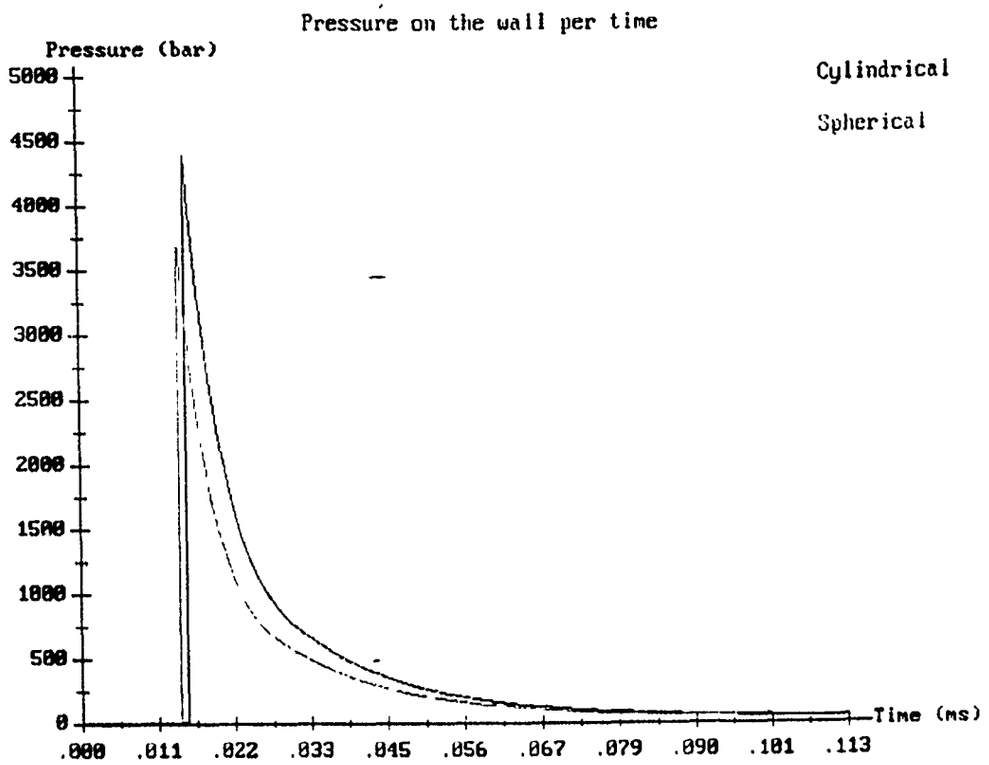
Pressure on the wall per time
Pressure (bar)
5000
4500
4000
3500
3000
2500
2000
1500
1000
500
0
Cylindrical
Spherical
Time (ms)
.000
.011
.022
.033
.045
.056
.067
.079
.090
.101
.113

Fig C.18

Tank wall breakup by internal pressure increase results

Loading on the wall

	Cylindrical	Spherical
Impulse per square (bar*s)	.031508	.026749
Dissipation per mass (kJ/kg)	33.1112	33.5926
Elastic energy per mass (kJ/kg)	94.7972	89.5447
Final density (g/cm^3)	2.1292	2.1175
Final velocity (m/s)	2580.6010	2172.9766
Loading time (ms):	.0590	.0666
Wall destruction time (ms):	.0337	.0366
Fragmentation occurs:	Yes	Yes

Press any key to continue

Fig. 6.19.

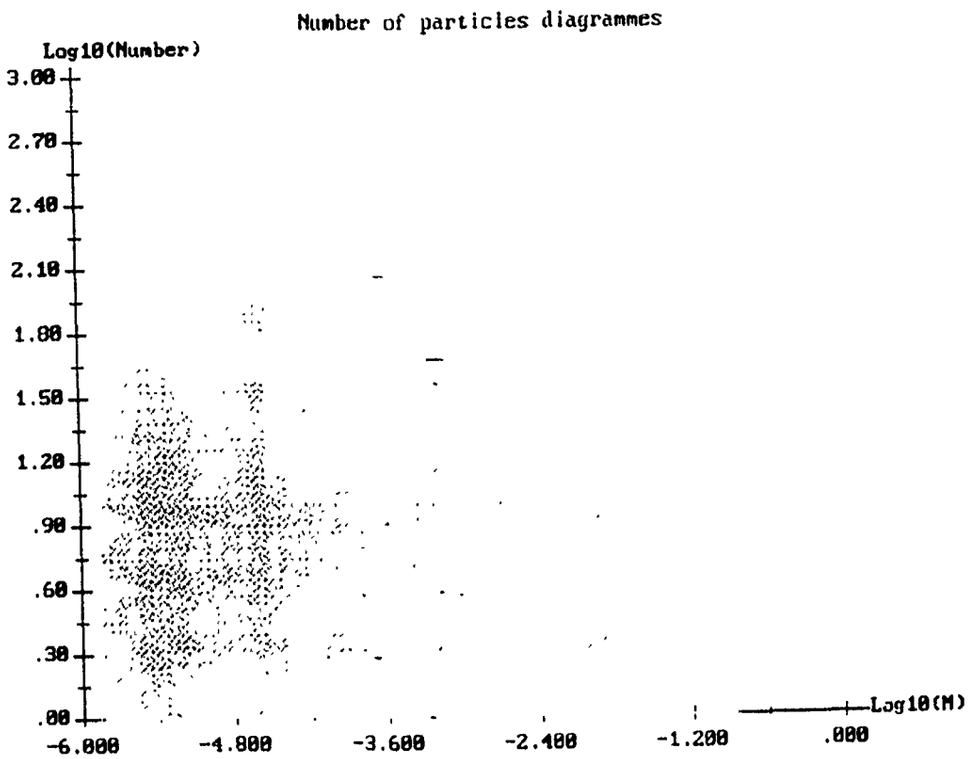
Number of particles diagrammes
Log10(Number)
3.00
2.70
2.40
2.10
1.80
1.50
1.20
.90
.60
.30
.00
-6.000
-4.800
-3.600
-2.400
-1.200
.000
Log10(M)

Fig [illegible]

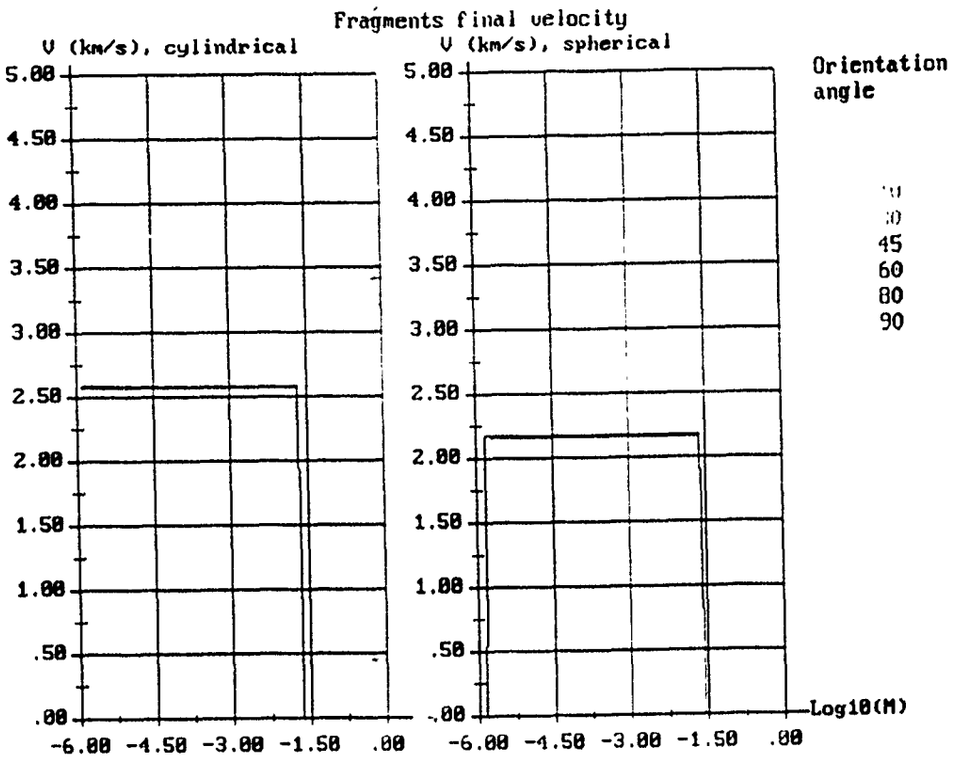
Fragments final velocity
V (km/s), cylindrical
V (km/s), spherical
Orientation angle
0
30
45
60
80
90
5.00
4.50
4.00
3.50
3.00
2.50
2.00
1.50
1.00
.50
.00
-6.00 -4.50 -3.00 -1.50 .00
Log10(M)

Fig. 21

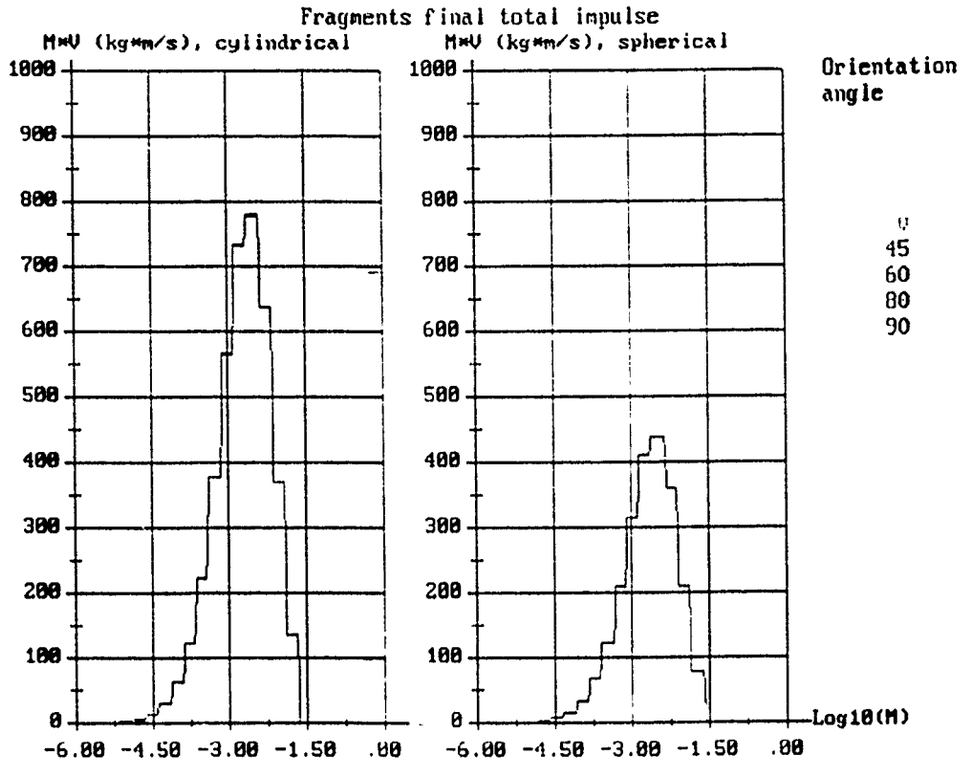
Fragments final total impulse
M*V (kg*m/s), cylindrical
M*V (kg*m/s), spherical
Orientation angle
0
45
60
80
90
1000
900
800
700
600
500
400
300
200
100
0
-6.00 -4.50 -3.00 -1.50 .00
Log10(M)

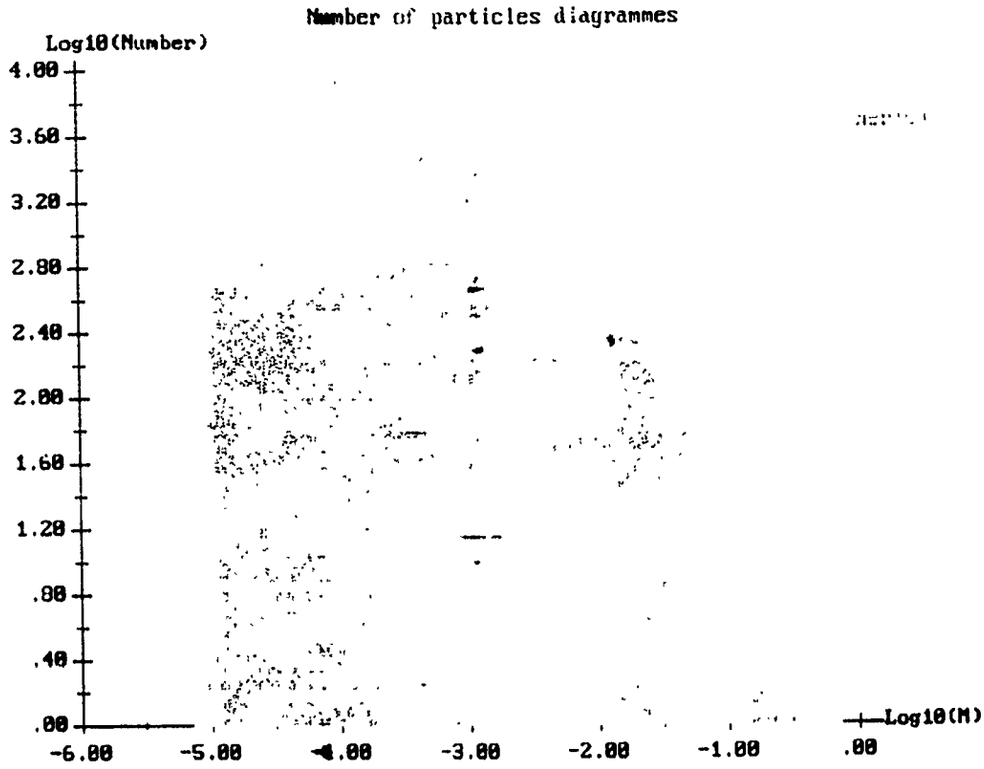
Number of particles diagrammes
Log10(Number)
4.00
3.60
3.20
2.80
2.40
2.00
1.60
1.20
.80
.40
.00
-6.00
-5.00
-4.00
-3.00
-2.00
-1.00
.00
Log10(M)

Fig. 6.23.

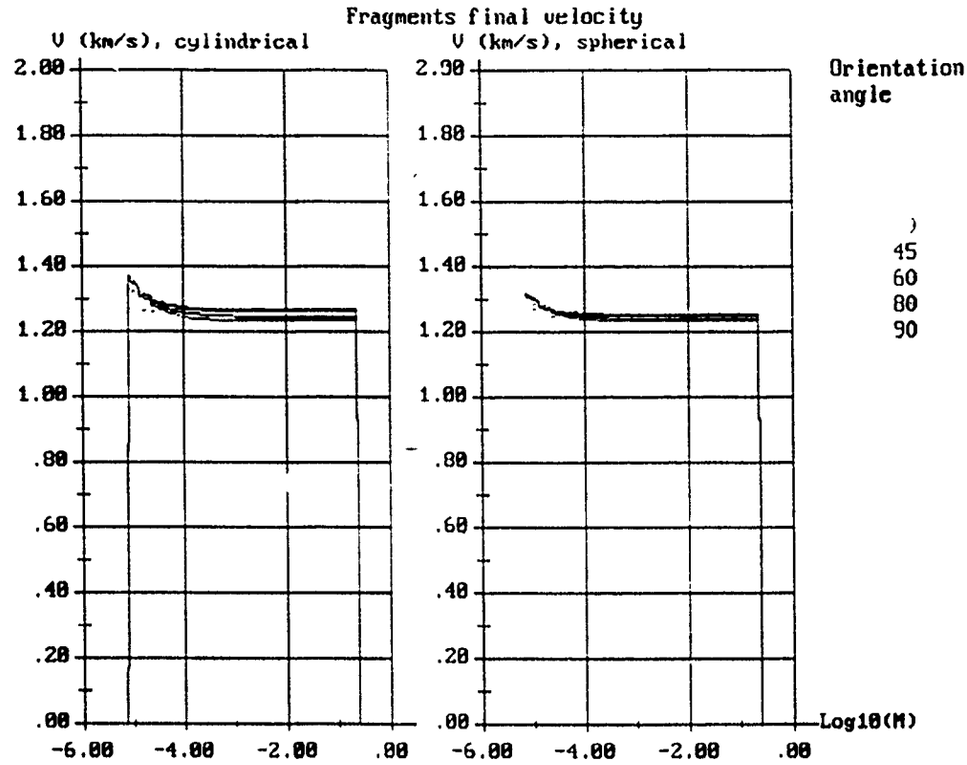
Fragments final velocity
V (km/s), cylindrical
V (km/s), spherical
Orientation angle
45
60
80
90
2.00
1.80
1.60
1.40
1.20
1.00
.80
.60
.40
.20
.00
-6.00
-4.00
-2.00
.00
Log10(M)

Fig 6.24

The program calculates prediction of fragments number, mass-number distribution, final velocities and momentum depending on combustion process in the closed vessel of simple shape – cylindrical with hemispherical edges. The theoretical part of calculation is described in the report.

The program requires IBM AT or compatible 386/87 or 486 with VGA/SVGA monitor. MSDOS ver.3.30 or higher and 640K memory.

Minimal set of files:
FTB.EXE - program itself
14FONT - font for graphic applications. In case of absence of this file the program in graphic modes will use default text character font but with less accuracy.

Extended set of files:
*.INI – user-named files containing initial data information.
*.RES – user-named files containing results of calculations.

Process of calculations description.

0. PRELIMINARY NOTES.

The program is controlled only by keyboard with no use of a mouse. To print results some external resident program is needed (such a program mostly uses <Print screen> key to be activated). If you want to take some printed copies from the plots you must run such a program before.

1. START.

To start the program, one should run FTB.EXE. After the first screen appears one can press <ESC> to exit immediately or any other key to enter the INITIAL MENU. If the file 14FONT doesn't exist or the system cannot access it or if there is less available memory than needed, then the warning message appears on screen:
- "Cannot access file or allocate memory for graphics font data"
Then the system anyhow changes to INITIAL MENU.

2. INITIAL MENU.

This menu contains 3 items:
DATA FROM FILE, INPUT DEFAULT DATA and EXIT TO DOS. Navigation between items is performed with <Right> and <Left> keys. To choose an item one should press <Enter> key. The <Esc> key here is inavailable. The primarily active item always is INPUT DEFAULT DATA.

2.1. DATA FROM FILE.

The system asks for the file name (without extension) where to use initial data from. Then it tries to open this file with .INI extension and to read initial data from it. If this file doesn't exist or the access is denied then the system says "Cannot access file" and remains in the INITIAL MENU. Else it reads the initial data and changes to INITIAL DATA

EDIT. Note that the filename then turns to be active

2.2. INPUT DEFAULT DATA.

The system just simply changes to INITIAL DATA EDIT. The active initial data (default or previously read from a file) gets a chance to be edited for new calculation.

2.3. EXIT TO DOS. (See FINISH).

3. INITIAL DATA EDIT.

At first the system opens a screen to edit the following list of data (first input screen):
- data on the chemical reaction stoichiometry: stoichiometric coefficients of the chemical reaction in the vessel, initial and final, for the set of generalized components – fuel, oxidizer, reaction product and neutral;
- data on the reagent's properties: molar masses, initial volumetric concentrations, initial adiabatic ratio and final adiabatic ratio;
- data on the reaction energetics and ignitivity: reaction heat release, activation energy, predetonational length, deflagration speed, unsteady detonation length, detonation formation length.

Purposes for this data are described in the report. To choose a field to edit one can use <Left>, <Right>, <Up>, <Down>, <Home> and <End> keys; note that <Left> and <Up> do the same as like as <Right> and <Down>. To begin editing a field press <Enter> or any other (no navigation's) key. To confirm editing and exit press <Esc> Then if some limitations are violated, a warning message appears on the screen, and editing continues. When a field is in the process of editing, <Left> and <Right> moves the cursor, <Del> and <Backspace> performes symbols deletion, <Enter> confirms and <Esc> breaks editing.

Limitations for the values edited on the first input screen produce the following warning messages in case of their violation:
- "Invalid data on reaction coefficients"
(stoichiometric coefficients must be non-negative);
- "No fuel on reaction's input"
(fuel stoichiometric coefficient before the reaction must be positive);
- "No products on reaction's output"
(products stoichiometric coefficient after the reaction must be positive);
- "Netral component can't change in reaction"
(neutral component stoichiometric coefficients before and after the reaction must be the same);
- "Invalid molar mass of a component participating the reaction"
(molar mass of each component with positive stoichiometric coefficient must be positive);
- "Negative or zero initial concentration of an input component"
(initial concentration of each component with positive stoichiometric coefficient before the reaction must be positive);
- "Adiabatic ratio of participating component must be from 1 to 1.67".
- "Molar mass of components must be the same both on input and output"
(total molar mass of components must be the same both before and after the reaction);

- "Sum of volumetric concentrations on input must be 1".
- "Negative or zero heat output: ignition can't occur"
(reaction's heat must be positive);
- "Negative or zero activation energy"
(activation energy must be positive);
- "Negative or zero predetonational length"
(predetonational length must be positive);
- "Negative or zero deflagration speed rate"
(deflagrational speed must be positive);
- "Invalid detonation's formation length"
(detonation's formation length must be positive but not exceeding predetonational length);
- "Invalid overdriven detonation's formation length"
(overdriven detonation's formation length must be positive but not exceeding detonation's formation length).

Then the system opens a screen to edit the following list of data (second input screen):
- data on initial internal conditions: pressure and temperature;
- data on geometry: fuel tank radius and length. Note that "length" here means total length of the vessel including hemispherical edges;
- data on the membrane wall geometry and thermodynamics: thickness, density, heat capacity and volume extendibility (with heating);
- data on the stresses modules and viscosity: shifting module, elasticity limit (initial), elasticity limit (maximal), dynamical viscosity of the wall material;
- data on Steinberg - Guinane model constants: 4 values depending on the wall material;
- data on destruction criterium: maximal dissipation, energy per breach square unit, characteristical square of fragments and exponential parameter in the distribution law.

All rules of editing are the same as for the first input screen.

Limitations for the second input screen produce the following warning messages in case of their violation:
- "Invalid initial pressure value"
(initial pressure must be positive);
- "Invalid initial temperature value"
(initial temperature must be not below 20K and above 5000K);
- "Fuel tank length must be equal or exceed two radii"
(to perform the vessel with a middle cylindrical part and two hemispherical edges);
- "Tank wall thickness less or equal to zero"
(thickness of the tank wall must be positive);
- "Wall density must be positive";
- "Wall heat capacity must be positive";
- "Wall thermal volume extendibility must be positive";
- "Wall shifting module must be positive";
- "Wall elasticity limit must be positive";
- "Maximal wall elasticity limit must exceed the initial one";
- "Wall dynamical viscosity must be positive";
- "Each of the Steinberg - Guinane model constants must be positive";

- "Maximal dissipation must be positive":
- "Energy for breaches origination must be positive":
- "Characteristical square of fragmentation must be positive":
- "Negative exponential parameter in fragmentation distribution"
(it must be positive or zero).

After confirming editing of the second input screen the system changes to the MAIN MENU.

4. MAIN MENU.

The MAIN MENU of the program consists of 9 items, change between them is performed with <Left>, <Right>, <Up>, <Down>, <Home> and <End> keys. Item is chosen with <Enter> key, <Esc> key is inavailable. When one enters the MAIN MENU from the INITIAL DATA EDIT, the initial item is CALCULATE. Items of the main menu are:
CALCULATE, NEW CALCULATION, EXIT TO DOS.
SHOW RESULTS, SAVE RESULTS, READ RESULTS.
SHOW INITIAL DATA, SAVE INITIAL DATA, SERVICE.

4.1. CALCULATE.

The system calculates results if the flag "calculated" is off. This flag is off on enter from INITIAL DATA EDIT and turns on after calculation or READ RESULTS (in case of succesful reading). When this flag is on, choosing of this item leads to warning message: "Results for the active initial data have been already obtained", and the choice pseudo-cursor in MAIN MENU turns to SHOW RESULTS. Calculation consists of three stages: internal process (deflagration, detonation, ddt-process or no process at all), wall [illegible]ing and fragmentation, final velocities calculation. If the flag "output during calculations" is on (it can be switched on/off in SERVICE), then after each stage temporary results will be displayed (all these results can also be displayed via SHOW RESULTS). By default the flag "output during calculations" is off.

4.2. NEW CALCULATION.

The system turns again to INITIAL MENU. Note that the flag "calculated" turns off, but the active initial data is conserved as well as the active filename.

4.3. EXIT TO DOS. (See FINISH).

4.4. SHOW RESULTS.

If the flag "internal details output" (see SERVICE) is on, then the system shows the following.

First screen of internal results.
- Concentrations of reagents;
- Volumetric initial concentrations;
- Mass initial concentrations;
- Volumetric final concentrations;
- Mass final concentrations;
- Molar masses of reagent mixtures (initial and final).

- Adiabatic ratio of mixture (initial and final):
- Reaction's heat release (per mol and per mass unit):
- Equilibrium final conditions (pressure and temperature):
- Type of the process inside the fuel tank (no process, deflagration, normal detonation, ddt in progress or ddt originating).

Second screen of internal results.
For spherical and cylindrical parts of the vessel the following is shown:
- Pressure (initial, before shock wave, after shock wave, after reaction zone, after shock's reflection, after reaction zone's reflection and final). In case of "no process" or "deflagration" only initial and final pressure values have resonable meaning.
- Detonation's wave velocity (for detonation or ddt process). - Time intervals (ignition – detonation origin, reaction zone near the wall duration, relaxation time, active pressure increase duration). Some intervals have resonable meaning only in detonation or ddt processes.

Third screen of internal process shows the chart of pressure-time evolution near the wall (in graphics mode). Data for cylindrical case is shown in white, for spherical – in red. If the curves are the same (i.e. when normal detonation occurs) the red curve is drawn over the white one.

If the flag "membrane burst details output" is on (see SERVICE) then the system shows the following.

First screen of membrane burst and loading output.
If no process in the vessel, then the system simply types "No chemical reaction in the vessel", else for spherical and cylindrical parts of the vessel the following results are displayed.
- Impulse per square:
- Dissipation per mass unit:
- Elastic energy per mass unit:
- Final density:
- Final velocity:
- Loading time (time of pressure application):
- Wall destruction time (in case of breakup it is usually less then the Loading time, otherwise it is zero, i.e. it has no reasonable meaning).
- If fragmentation occurs (yes or no).
Note that the first four values are calculated until the breakup occurs or the conditions show that it will not occur; the 5th (final velocity) value in case of breakup relates to the moment when the huge increase of pressure near the wall will relax and the fragments then will accelerate mostly by the drag forces.

Second screen of membrane burst and loading output.
Shows diagrammes of mass-number distribution of fragments for cylindrical case (in gray) and spherical case (in dark red). If the diagrammes for both cases transect then one will see them in pink. Diagrammes are shown in graphics mode in logarithmic axes.

If the flag "final velocities output" is on (see SERVICE) then the system shows the following.

First screen – final velocity depending on fragment's mass plots for cylindrical and spherical cases are shown. Different curves relate to different orientation angles of fragments: they are shown in different colors, and the corresponding angles are shown in the right part of the screen each in its own color. If no fragmentation occurs for some case (cylindrical, spherical or both of them) then "No fragmentation" is typed instead of a plot.

Second screen - final momentum of fragments depending on mass plots for cylindrical and spherical cases are shown. Different curves relate to different orientation angles of fragments like on the previous screen.

Note that change between screens is made by pressing a key.

4.5. SAVE RESULTS.

This item of the MAIN MENU works when "calculated" flag is on and the active filename is determined. Then the results are saved into file named <filename>.res. Otherwise the following messages can appear on screen:
- "Results on the active initial data haven't been obtained"
(the flag "calculated" is off);
- "Cannot access file, write initial data at first"
(filename is undefined or cannot open file with defined name).

4.6. READ RESULTS.

This item of the MAIN MENU works when the active filename is determined. Then the results are read from file named <filename>.res. Otherwise the following message can appear on screen:
- "Cannot access file"
(filename is undefined or cannot open file with defined name).
Note that succesfull pass through this item of the MAIN MENU sets "calculated" flag on.

4.7. SHOW INITIAL DATA.

The active initial data is shown in the order described above in INITIAL DATA EDIT, but editing is now unavailable.

4.8. SAVE INITIAL DATA.

The system asks for the file name (without extension). The active filename is default if determined. Then it tries to open a file named <filename>.ini and to save initial data into it. If opening file is unsuccesfull then a warning message appears:
- "Cannot access file".
Note that in case of succesfull write to file the active filename is (re)determined.

4.9. SERVICE.

This item of the MAIN MENU leads to sub-menu consisting of five items:
- "Proceed (Bypass) internal details output".

- "Proceed (Bypass) membrane burst details output".
- "Proceed (Bypass) final velocities output".
- "Proceed (Bypass) output during calculations".
- "Exit to main menu".

Each of the first four items serves to switch on/off the corresponding control flag, the status of each flag is shown in the prompt (i.e. if "Proceed" is in the prompt then the flag is on). The purposes of these flags can be seen above in CALCULATION and SHOW RESULTS. One can exit to main menu using the 5th item or just pressing the <ESC> key. Note that if the three first flags are OFF then SHOW RESULTS will not show any results at all.

5. FINISH.

The first screen appears again, but with "Press any key to exit" on it. Then after a key is pressed the program exits to DOS.